Applied Surface Science 441 (2018) 588–598

Contents lists available at ScienceDirect

Applied Surface Science

journal homepage: www.elsevier.com/locate/apsusc

Full Length Article

Sensing properties of pristine boron nitride nanostructures towards alkaloids: A first principles dispersion corrected study

Basant Roondhe [a], Shweta D. Dabhi [b], Prafulla K. Jha [a,*]

[a] Department of Physics, Faculty of Science, The Maharaja Sayajirao University of Baroda, Vadodara 390 002, India
[b] P. D. Patel Institute of Applied Sciences, Charotar University of Science and Technology, CHARUSAT-Campus, Changa 388 421, India

ARTICLE INFO

Article history:
Received 1 December 2017
Revised 22 January 2018
Accepted 27 January 2018
Available online 2 February 2018

Keywords:
Boron nitride nanostructure
Alkaloids
Electronic properties
Binding energy
Quantum conductance
Sensors

ABSTRACT

To understand the underlying physics behind the interaction of biomolecules with the nanomaterials to use them practically as bio-nanomaterials is very crucial. A first principles calculation under the frame work of density functional theory is executed to investigate the electronic structures and binding properties of alkaloids (Caffeine and Nicotine) over single walled boron nitride nanotube (BNNT) and boron nitride nanoribbon (BNNR) to determine their suitability towards filtration or sensing of these molecules. We have also used GGA-PBE scheme with the inclusion of Van der Waals (vdW) interaction based on DFT-D2. Increase in the accuracy by incorporating the dispersion correction in the calculation is observed for the long range Van der Waals interaction. Binding energy range of BNNT and BNNR with both alkaloids have been found to be −0.35 to −0.76 eV and −0.45 to −0.91 eV respectively which together with the binding distance shows physisorption binding of these molecules to the both nanostructures. The transfer of charge between the BN nanostructures and the adsorbed molecule has also been analysed by using Lowdin charge analysis. The sensitivity of both nanostructures BNNT and BNNR towards both alkaloids is observed through electronic structure calculations, density of states and quantum conductance. The binding of both alkaloids with BNNR is stronger. The analysis of the calculated properties suggests absence of covalent interaction between the considered species (BNNT/BNNR) and alkaloids. The study may be useful in designing the boron nitride nanostructure based sensing device for alkaloids.

1. Introduction

In recent years, boron nitride nanostructures (BNNs) including nanotube, nanoribbon and nanosheet have attracted extensive attention from many experimental and theoretical groups [1–4]. BNNs are promising materials for nano electronics, bio sensing, drug delivering and medical applications due to their extensive properties like high temperature stability, low dielectric constant, large thermal conductivity and oxidation resistance [5–10]. Boron nitride exists in cubic BN (c-BN), trigonal BN, wurtzite BN (w-BN) and hexagonal BN (h-BN) isomers with significant attention to h-BN [11].

The BNNs have distinct differences or advantages compared to those of their carbon counterpart due to their polar character [12]. The large intrinsic bandgap arising from the ionic nature of bonds and their nontoxicity make them more suitable over carbon nanostructure to be used in bio applications [13]. The modulation of the band gap can be easily achieved in the case of boron nitride nanoribbon (BNNR) in contrast to its carbon counterpart graphene nanoribbon (GNR) [14,15]. The BNNR structurally similar to GNR is classified in two configurations: (a) zigzag BNNR (ZBNNR) and (b) armchair BNNR (ABNNR) [16–18]. The literature reveals diverse and unconclusive results on width dependent properties of both ribbons [17–19]. While Du et al. [17] show a decrease in the band gap of ZBNNR with increase in the ribbon width, an oscillatory behaviour for the width dependent bandgap is observed for ABNNR [20]. There have been several theoretical and experimental studies to understand the interaction of boron nitride nanotube (BNNT), BN monolayer and BNNR with a range of biomolecules [21–24]. Tremendous efforts are still under development to evaluate and modulate the bio compatibility of BNNs to further improve its biological and medical applications [25–28].

Caffeine and nicotine biomolecules which belong to alkaloid family and are therapeutic molecules [29,30] mainly used for medical purposes can be obtained from coffee and tobacco. These molecules serve as stimulants for central nervous system in human body. They show positive effect on human if consumed in proper quantity but can be disastrous in the case of heavy consumption. It is a heavily addictive drug and can have side effects such as high

* Corresponding author.
E-mail addresses: prafullaj@yahoo.com, pk.jha-phy@msubaroda.ac.in (P.K. Jha).

https://doi.org/10.1016/j.apsusc.2018.01.249
0169-4332/

heart rate, high blood pressure and insomnia [31]. The use of caffeine has been started in energy drinks to provide physical stimulation and hence face ban on sale and or production in many countries. Therefore the fabrication of nanostructure based sensors and filters to absorb these chemicals are in progress. Recently, using carboxylated carbon nanotube (CNT) as an additive in filter tip to increase nicotine and tar sorption has been realized experimentally [32].

A theoretical study using density functional theory (DFT) on the interaction of nicotine molecule with single walled CNT is reported by Girao et al. [33]. Lee and co-workers [34] reported a non-covalent interaction of CNT with nicotine and caffeine through π-staking. However, both studies report a different binding geometry and binding energies. It is found that the BNNT which exhibits similar mechanical properties and thermal conductivity as CNT is more resistive towards oxidation than CNT due to better chemical stability in the case of former [35–37]. The strong chemisorption of caffeine and nicotine molecules on two types of boron nitride nano cages $B_{12}N_{12}$ and $B_{16}N_{16}$ is reported [38]. $B_{12}N_{12}$ cage is found better for the adsorption of caffeine and nicotine molecules. The binding geometry, binding energies and electrical conductance of BN nanocages are modified over the interaction of HCN and methanol molecules [39,40]. In addition, to understand the nature of binding between BNNT with nucleobases of DNA – RNA and amino acids and effect of adsorption of these biomolecules on the transport properties of BNNT few DFT studies are reported in literature [41,42]. Though the authors of these studies were successful in bringing the nature of interaction and possible use of these combinations for biosensors applications but ignored the important contribution of Grimme's dispersion despite being them as weakly bound systems of vdW interactions. The adsorption and electronic properties of boron nitrides are highly dependent on the extent of

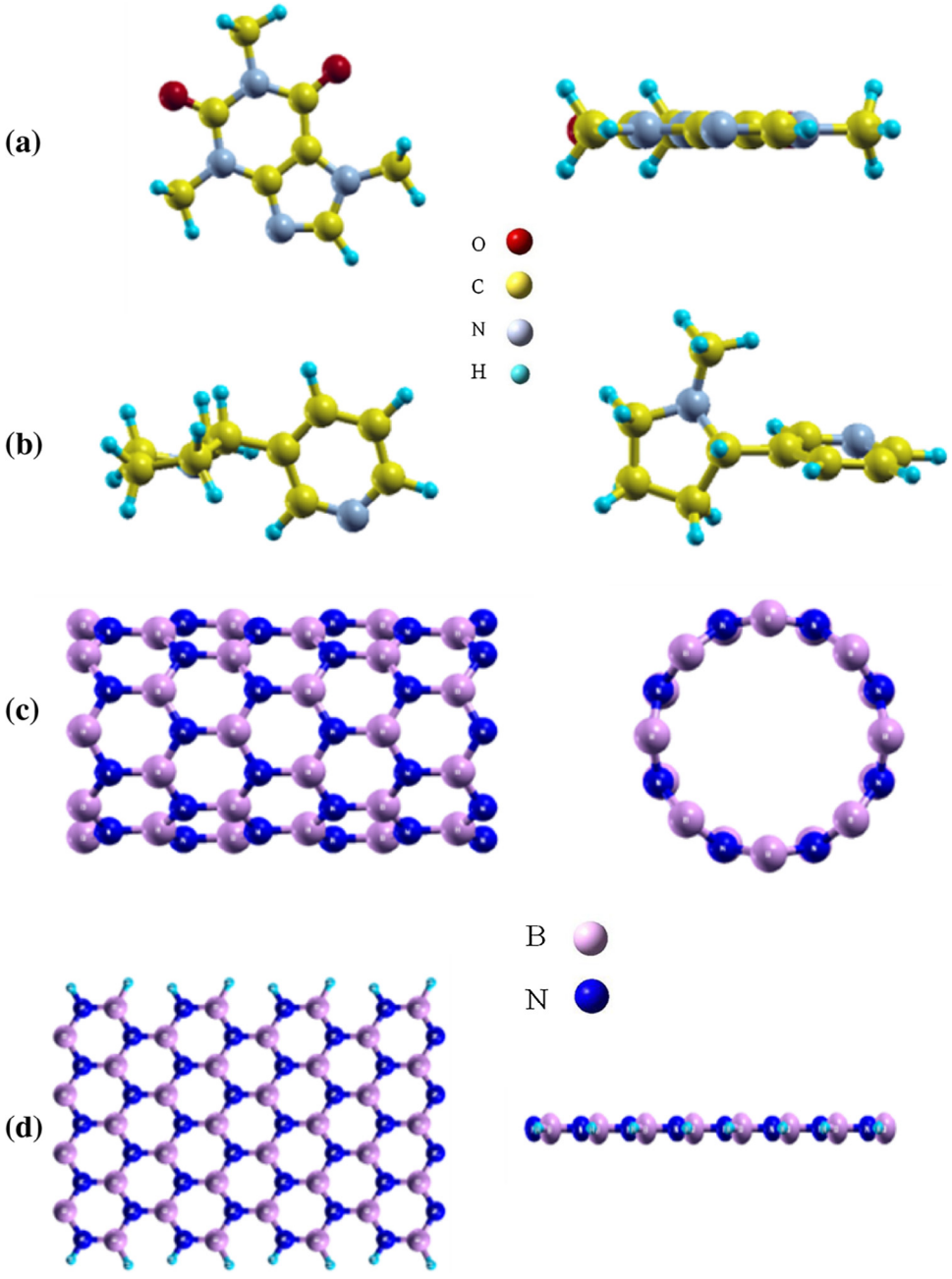

Fig. 1. Optimized structures of (a) Caffeine, (b) Nicotine, (c) Pristine boron nitride nanotube and (d) Pristine boron nitride nanoribbon. The figure also shows the side view of optimized structures.

confinement, arrangement of atoms and length. A study on the interaction of biomolecules, alkaloids, nucleobases, etc. is yet to be carried out for BN nanoribbons. In the present work, our main motivation is to identify the factors influencing the interaction of caffeine and nicotine with BN nanotube and BN nanoribbon using first principles based density functional theory calculation with the incorporation of dispersion corrections to account vdW interactions.

2. Computational methods

All calculations in the present study are performed by employing the plane wave pseudopotential approach proposed by Perdew-Burke-Ernzerhof within the Generalized Gradient Approximation (GGA) [43] for exchange correlation functional as implemented in the Quantum espresso code [44]. The single particle functions are expanded in a plane wave basis set up to kinetic energy cut off and charge density are 80 Ry and 800 Ry respectively which is sufficient to fully converge the lattice parameters and total energy. Brillouin zone integrations are performed using $1 \times 1 \times 8$ and $1 \times 16 \times 1$ Monkhorst and Pack [45] special point grids for BNNT and BNNR respectively. The system have been fully relaxed to obtain the ground state structure with residual forces less than 0.001 eV/Å. The average B—N bond length in the optimized configuration of the pristine BNNT and BNNR is 1.48 Å. A comparative analysis of two alkaloids i.e. caffeine and nicotine

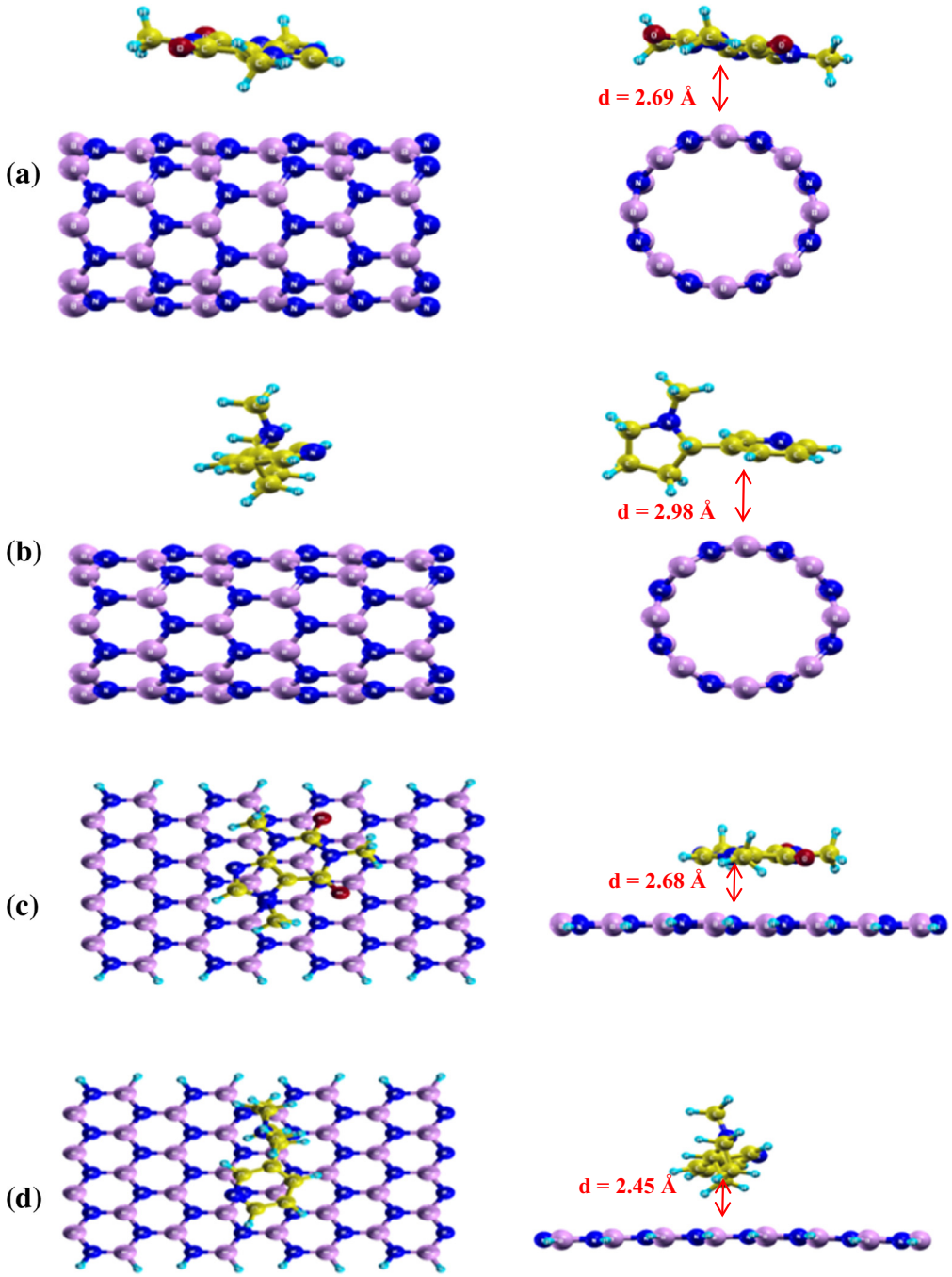

Fig. 2. Equilibrium geometry of physisorbed Caffeine and Nicotine molecules on (a and b) BNNT and (c and d) BNNR. The figure also shows the side view of optimized structures of functionalized BN nanostructures with alkaloids.

interaction with both BNNT and BNNR has been carried out by full structure optimization, adsorption energy, electronic structure and density of states (DOS). It has been emphasized in the literature that a precise quantum mechanical description of interaction of molecules with nano surface requires accounting for dispersion forces particularly for weakly bound systems [46]; therefore it is important to choose a suitable computational method that should consider the correct description of long-range electron correlation. The present study shows the comparative result with and without the employment of Grimme's dispersion correction [47] to incorporate the long distance van der Waals interaction between the adsorbent and the adsorbate. The adsorption energy E_{ad} has been calculated according to the equation as follows

$$E_{ad} = E_{BNN+alkaloid} - (E_{BNN} + E_{alkaloid}) \quad (1)$$

where $E_{BNN+alkaloid}$ is the total energy of BNNs (BNNT and BNNR) adsorbed by alkaloid (caffeine or nicotine), E_{BNN} is the total energy of the adsorbent nanostructure (BNNT or BNNR), $E_{alkaloid}$ is the total energy of alkaloid (caffeine or nicotine) obtained from their fully optimized geometries. According to the definition $E_{ad} < 0$ indicates the exergonic nature of the adsorption. The quantum conductance has also been calculated at zero bias using the Landauer formalism [48], using maximally localized Wannier functions (MLWF) basis as implemented in the Wannier90 code [49].

3. Results and discussion

To understand the interaction of alkaloids (caffeine and nicotine) with two boron nitride nanostructures; (zigzag) BNNT and

Table 1
Calculated HOMO energies, LUMO energies, energy band gap (E_g), adsorption energy (E_{ad}), Fermi level energies (E_f) and distance of the molecule over BNNT and BNNR (d).

System		HOMO (eV)	LUMO (eV)	E_g (eV)	E_{ad} (eV)	E_f (eV)	d (Å)
Without dispersion	BNNT	−4.4285	−0.8656	3.563	–	−2.647	–
	Caffeine	−5.2272	−1.7121	3.515	–	−3.469	–
	Nicotine	−4.9027	−1.5005	3.402	–	−3.201	–
	BNNT + Caffeine	−3.6309	−0.5969	3.034	−0.030	−2.113	3.6
	BNNT + Nicotine	−3.2974	−0.6331	2.664	−0.025	−1.965	2.99
With dispersion	BNNT	−4.4310	−0.8671	3.563	–	−2.649	–
	Caffeine	−5.2273	−1.7122	3.515	–	−3.469	–
	Nicotine	−4.9027	−1.5005	3.402	–	−3.201	–
	BNNT + Caffeine	−3.6185	−0.6199	2.999	−0.76	−2.119	2.69
	BNNT + Nicotine	−3.3442	−0.6264	2.718	−0.35	−1.985	2.98
	BNNR	−4.5328	0.0234	4.556	–	−3.726	–
	BNNR + Caffeine	−3.8187	−0.3484	3.470	−0.91	−2.401	2.68
	BNNR + Nicotine	−3.5103	−0.1156	3.395	−0.48	−3.385	2.45

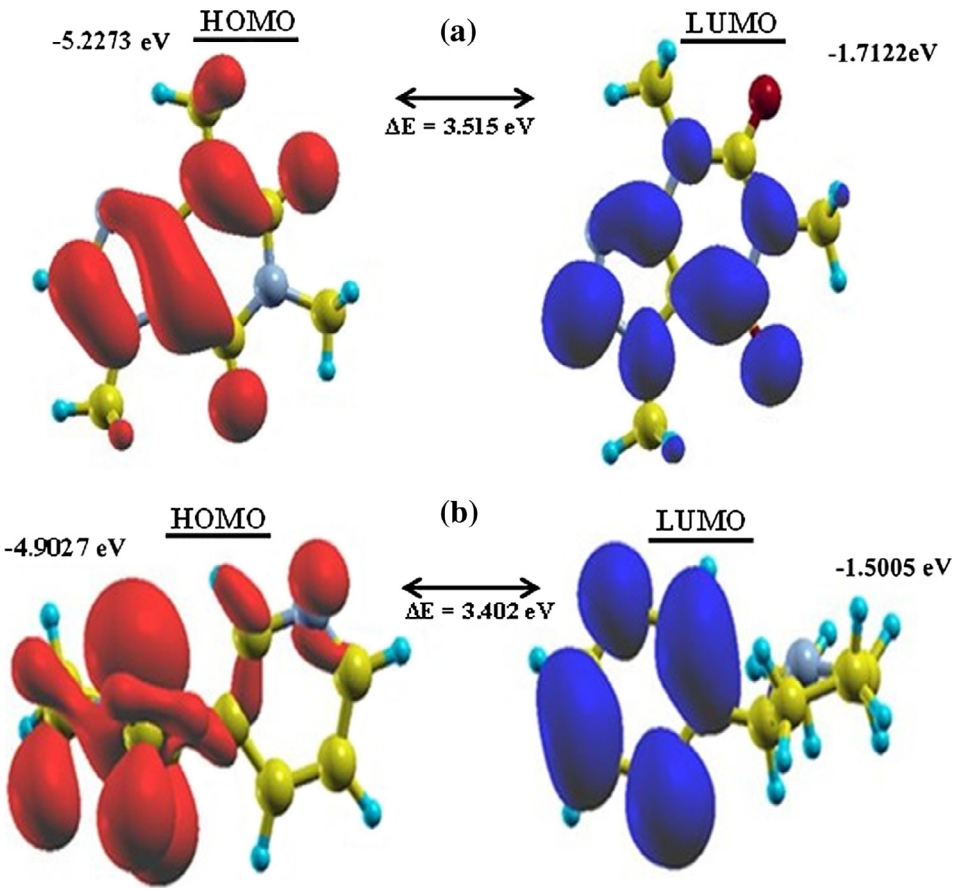

Fig. 3. HOMO (red) and LUMO (blue) of (a) caffeine molecule and (b) nicotine molecule. (For interpretation of the references to color in this figure legend, the reader is referred to the web version of this article.)

(armchair) BNNR, we first individually optimized the structures of BNNT, BNNR, caffeine and nicotine which are presented in Fig. 1(a–d). The diameter of BNNT (8,0) and width of BNNR obtained after optimization is 6.40 Å and 10.03 Å respectively. Fig. 2(a–d) presents the optimized geometries of caffeine and nicotine molecules adsorbed over BNNT and BNNR. Various orientations were explored not only by changing the orientation of molecules (parallel and perpendicular) but also the distance between nanostructures and molecules before concluding the best optimized geometries. It is found that the molecules are weakly adsorbed in the case of perpendicular orientation due to less number of atoms of molecule facing the BN nanostructures and hence resulting into the low binding of molecules. As far as distance is concerned, nature of force between BN nanostructures and molecules is repulsive for close distance due to positive binding energy. However, the adsorption is maximum at 2.69 Å and 2.98 Å for caffeine and nicotine respectively which again gradually decreases and finally reduces to zero at 6 Å. The BNNT and BNNR facing hetero-atoms of caffeine and nicotine molecules show the most favourable orientation for adsorption. Fig. 2(b) clearly depicts that the nicotine

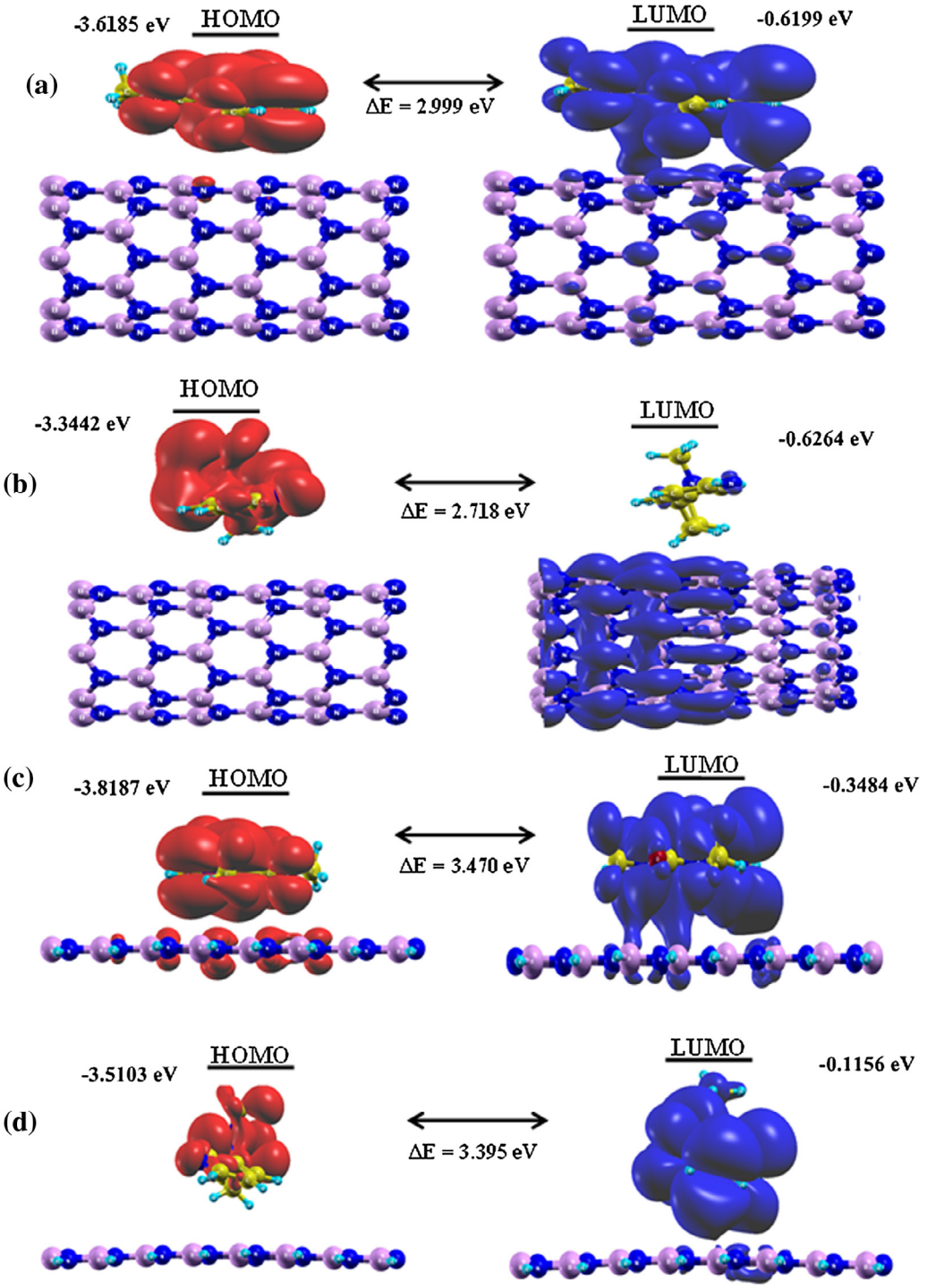

Fig. 4. HOMO (red) and LUMO (blue) of functionalized BNNT (a and b) and BNNR (c and d) with caffeine molecule and nicotine molecule. (For interpretation of the references to color in this figure legend, the reader is referred to the web version of this article.)

molecule prefer it's six member ring to be in contact with BNNT rather than its five member ring similar to the CNT [34] while in the case of BNNR both rings interact to the surface of BNNR due to available large surface for interaction (Fig. 2(c and d)).

Table 1 presents the calculated energy gap (E_g), adsorption energy (E_{ad}), Fermi energy (E_f), Highest occupied molecular orbital (HOMO) and Lowest unoccupied molecular orbital (LUMO) energies and distance of the alkaloid molecules from BNNT/BNNR without and with dispersion corrections. An effect of dispersion on the listed properties is clearly seen. The HOMO-LUMO gap for caffeine and nicotine molecules is 3.515 eV and 3.402 eV respectively which are in good agreement with the previous studies [34–38]. In caffeine the HOMO and LUMO wave functions are distributed over whole molecule as can be seen from Fig. 3(a). Fig. 3(b) shows that the HOMO of nicotine is dominating at its five member ring but the electron density is high at the phenyl group in LUMO. Fig. 4(a–d) shows HOMO and LUMO of alkaloids non-covalently adsorbed over BNNT and BNNR respectively. As shown in Table 1 the change in HOMO and LUMO energies due to adsorption of caffeine and nicotine over both BN nanostructures are in range of 0.71–1.0 eV and 0.35–0.48 eV respectively.

The total charge density of the caffeine and nicotine adsorbed on BNNT and BNNR is also calculated and presented in Fig. 5(a and b). Difference of individual atomic charges before and after adsorption of caffeine/nicotine on BNNs is less than 0.02e indicating no significant charge transfer between BNNs and alkaloids after adsorption.

The adsorption of both the alkaloid molecules are physical (physisorption) in nature as the distance between the molecules and considered BN nanostructures is large (Table 1). The inclusion of Grimme's dispersion significantly affects the binding energy of alkaloids with BN nanostructures. We do not present the parameters for pristine BNNR and adsorbed BNNR without dispersion. The binding energy without dispersion correction is quite low for alkaloids over BNNT suggesting endergonic adsorption. However, the inclusion of long range van der Waals interactions via dispersion corrected DFT operations turns adsorption into the physical adsorption. The calculated binding energy shows strong physisorption for caffeine over BNNT while comparatively a weak physisorption for nicotine even after the incorporation of the dispersion correction. The value of adsorption energy via π stacking for BNNT is almost half for nicotine adsorbed BNNT than caffeine adsorption. This means that the caffeine interact strongly to BNNT similar to the CNT [34]. This is quite consistent with the earlier study on the nicotine adsorption over CNT [33] which confirmed that the nicotine binds through physisorption until the CNT is defected and nicotine is covalently bounded to defected site [33].

Our calculations depict a dominance of BNNR over BNNT in the adsorption of alkaloids (caffeine and nicotine). The calculated binding energies over BNNR for caffeine and nicotine are −0.91 eV and −0.48 eV respectively which are more than the BNNT. This can be attributed to the higher sensitive semiconductive nature of BNNR [11]. Furthermore, the distance between caffeine and BNNT is d ∼ 2.6 Å. The distance is 2.45 Å and 2.68 Å respectively for nicotine and caffeine over BNNR. It is noteworthy that the inclusion of vdW interaction changes this distance more for caffeine than nicotine which can be attributed to the planer structure and aromatic rings of caffeine which allow large area for interaction between BN nanostructures and molecules [50,51]. It is noteworthy that the Dabbichi et al. [52] found binding energy for anthracene over CNT as 1 eV with the inclusion of dispersion. Furthermore, the adsorption energy is obtained in the range of 0.29–0.42 eV for five nucleobases with local density approximation (LDA) calculations by Mukhopadhyay et al. [53]. They have pointed out that their LDA calculations take care of dispersion and is equivalent to the GGA + vdW level of theory. The difference in the nature of interaction and binding energy of these alkaloids with the BNNT and BNNR can be explained on the basis of fundamentals of van der Waals forces that are directly proportional to the size and mass of the interacting molecules [54]. After the inclusion of an explicit dispersion correction term, it is evident that the adsorption is accompanied by the release of a large amount of energy and is driven by long range interactions. This observation emphasizes the role of van der Waals interactions in the adsorption process.

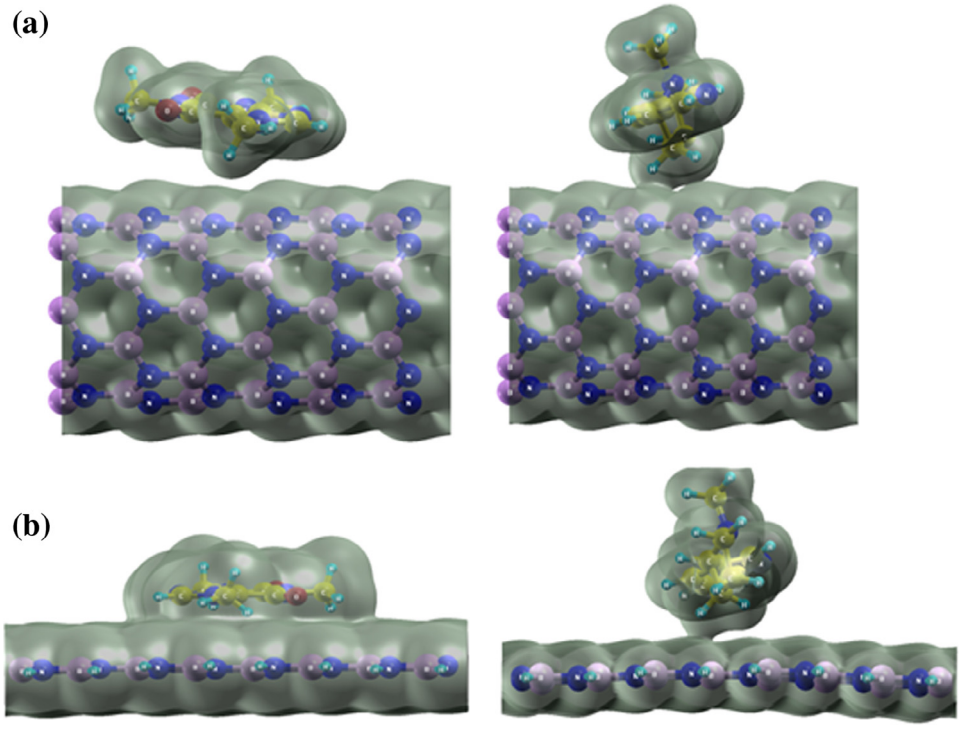

Fig. 5. Total charge density plot of BNNT and BNNR conjugated with Caffeine and Nicotine (a) BNNT and (b) BNNR. Isosurface levels were set at 0.09 bohr^{-3}.

The caffeine and nicotine molecules are physisorbed over BNNT and BNNR due to the large nearest atom distance (d ~ 2.6 Å) which make sure the elimination of any possibility of covalent bond formation. The physical nature of adsorption offers advantages in terms of easy removal and reusability of nanostructure, with no structural or electronic change in the adsorbate and adsorbent. The dispersion correction does not directly alter the wave function as it is considered herein as add-on term. However, significantly better stabilized geometries are obtained after optimization with the inclusion of dispersion correction. Furthermore, the adsorption energy calculated without dispersion correction deemed the process to be endergonic; it implied that the interaction is not favourable electronically.

It is also important to comment on the importance of BNNT/BNNR over another BN nanostructure systems. BN nanocages for biomolecular adsorption applications as the adsorption energies in both cases are comparable. Our study suggests the physisorption of alkaloid molecules over both BNNR/BNNT, which is good for a sensitive sensor as due to the physisorption the recovery as well as response time is much faster [55]. But in case of BN cage the chemisorption is occurring due to covalent and ionic bonds generated between the molecule and the cage. As we know chemisorption need some external energy due to which it increases the response as well as recovery time, which is big drawback for making sensor. In addition chemisorption process is normally irreversible.

To further understand the effect of alkaloids adsorption over the BNNT and BNNR, we present total electronic density of states (DOS) of caffeine, nicotine, BNNT, BNNR and functionalized BNNT and BNNR with caffeine and nicotine in Fig. 6(a–d). The projected

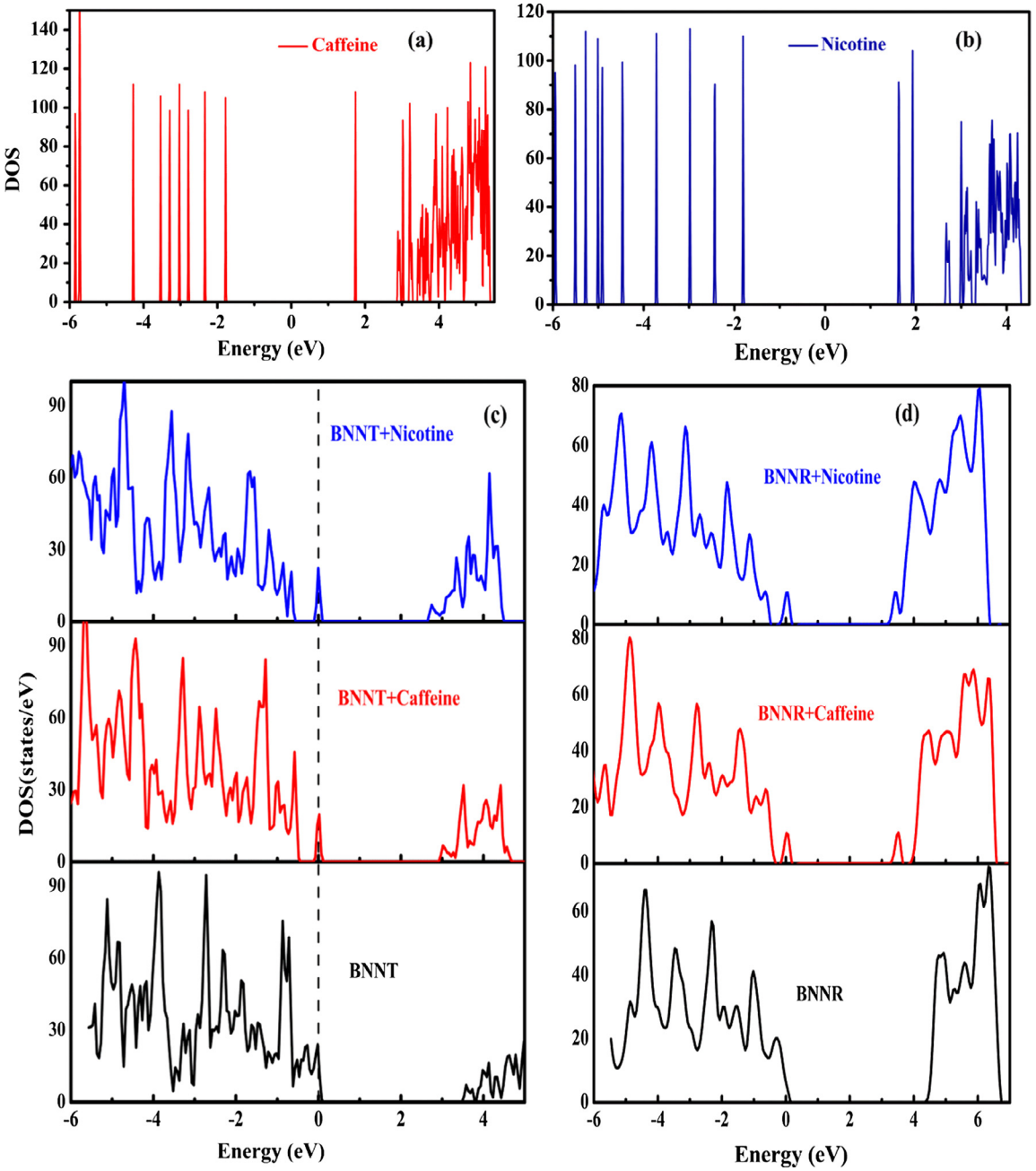

Fig. 6. Total DOS of (a) caffeine molecule, (b) nicotine molecule, (c) pristine and alkaloid (nicotine and caffeine) conjugated BNNT and (d) pristine and alkaloid (nicotine and caffeine) conjugated BNNR .

DOS (PDOS) for the pristine BNNT and BNNR and the caffeine and nicotine adsorbed over BNNT and BNNR are shown in Fig. 7(a–f). These figures clearly show that the alkaloid molecules modulate electronic properties of BNNT and BNNR. The analysis of DOS together with the PDOS indicates that the contributions of caffeine and nicotine molecules are localized around the top of the valance band. The DOS plots and the bandgap in the pristine boron nitride nanostructures clearly resemble the corresponding electronic band structures (not shown here). The PDOS plots of BNNT and BNNR presented in Fig. 7(a–f) shows that the B(2p) and N(2p) orbitals have major contribution in the conduction and valance bands respectively while the low lying electronic N(2s) and B(2s) orbitals do not contribute significantly. The PDOS due to H(1s) orbital arises due to passivation of the dangling bonds in BNNR. In pristine BNNT the valance band or HOMO states are closer to the Fermi level compared to LUMO which makes easy contribution for HOMO states to the Fermi level [53]. The density of states of caffeine and nicotine clearly shows the molecule like spectra with sharp peaks

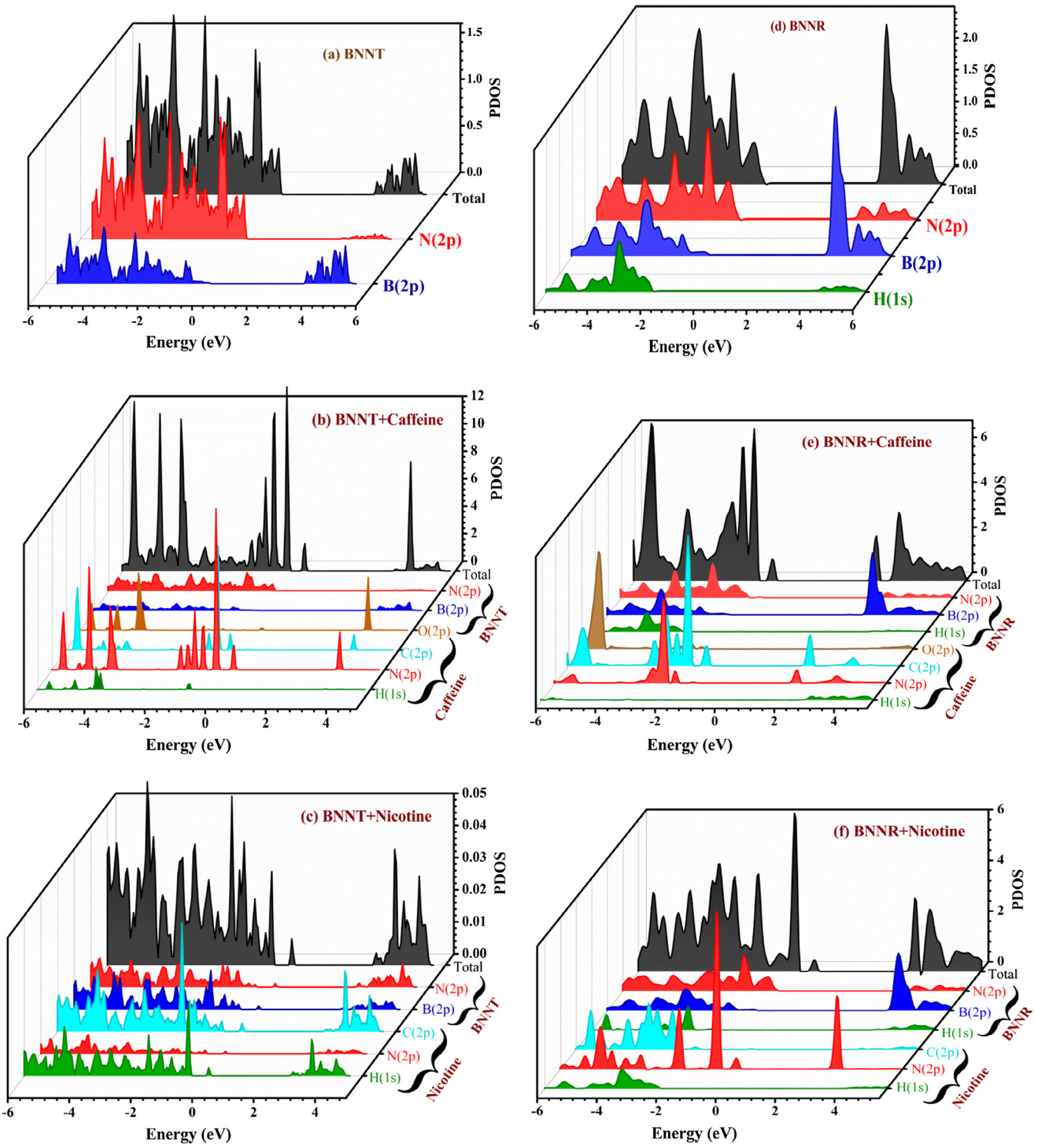

Fig. 7. PDOS of (a) pristine BNNT, (b) conjugated BNNT with caffeine, (c) conjugated BNNT with nicotine, (d) pristine BNNR, (e) conjugated BNNR with caffeine, (f) conjugated BNNR with nicotine,

mainly arising due to flat bands in band structures. The bandgap is almost same in both molecules. Now we turn our attention to the alkaloid adsorbed BNNT and BNNR. Fig. 6(c and d) shows that the adsorbed alkaloid molecule modifies the DOS of pristine BNNT and BNNR. The conduction band region corresponding to the LUMO moves towards Fermi level for both alkaloids. However, the valence band region corresponding to HOMO behaves differently in the case of both alkaloids. There is a large shift for HOMO away from Fermi level in caffeine and nicotine adsorbed BNNR. It is noteworthy that the adsorption of both caffeine and nicotine reduces the bandgap of considered BN nanostructures. The alkaloids adsorbed BNNR has wider bandgap than BNNT which is quite obvious due to larger bandgap of BNNR than BNNT. Comparatively larger change in band gap is observed after adsorption of alkaloids over BNNR than BNNT. Further, the DOS plots depict the presence of impurity states in the conduction band regions within HOMO-LUMO of pristine BNNT and BNNR arising due to the caffeine and nicotine molecules. Hence, alkaloids seem to be an active unit which affects electron mobility upon adsorption on to the BNNs. The present result confirms the binding energy analysis that the nicotine and caffeine molecules get physically adsorbed on the BN nanotube as well as nanoribbon. However, BNNR is found more dominant than BNNT for the adsorption of alkaloids; by these results and the previous study it is clear that BN nanostructures shows inert behaviour which does not affect the carrier molecules properties and hence it is good candidate for biomedical applications. Therefore BNNR is a good candidate for molecule carrier and should be explored more for its bio medical applications.

The quantum conductance which is calculated to study the quantum transport of charge and judge the modification in the electronic conductance of host adsorbate on interaction. This also help to understands or confirm the electronic DOS and possible charge transfer. Fig. 8 displays the calculated quantum conductance (G/G_0) using Wannier function [48,49] for pristine and alkaloids adsorbed boron nitride nanostructures BNNT and BNNR. The calculated quantum conductance shows the typical step by step like behaviour with each step corresponding to the sharp Van – Hove singularity of the density of states. The change in conductance can be attributed to the different electronic DOS at the Fermi level for caffeine, nicotine and BN nanostructures. Fig. 8(a and b) shows that the conductance of functionalized BNNT and BNNR is close to the superposition of that of a considered pristine BN nanostructures and alkaloids. This supports the conclusion drawn from adsorption and DOS that there is no significant charge transfer between BN nanostructures and alkaloids. However, a shift in peaks in comparison to pristine BNNT and BNNR is observed. The shift is prominent for nicotine indicating that the BN nanostructures can sense nicotine better than caffeine as well as distinguish each other. This suggests an interaction between the alkaloids and BN nanostructures despite no significant bonding or charge transfer between them.

For the calculation of quantum conductance we have used the same system to describe the leads and the scattering region. We find that the quantum conductance of the adsorbed BN nanostructure systems differs from pristine BN nanostructure. The quantum conductance of the alkaloid adsorbed BN nanostructures lies very close to the superposition of the pristine BN nanostructures even at other injection energies. Of course there exist characteristic features of the biomolecule (caffeine and nicotine) interaction with BN nanostructures in the form of dips in conduction curve. The similar conclusion is drawn from the sulphur chain encapsulated inside CNT [56]. Thus, our calculations provide solid support for the conclusion that both the nicotine and caffeine molecule modify the electronic conductance of BNNT and BNNR and introduces new conduction channels in the adsorbed biomolecule BN system.

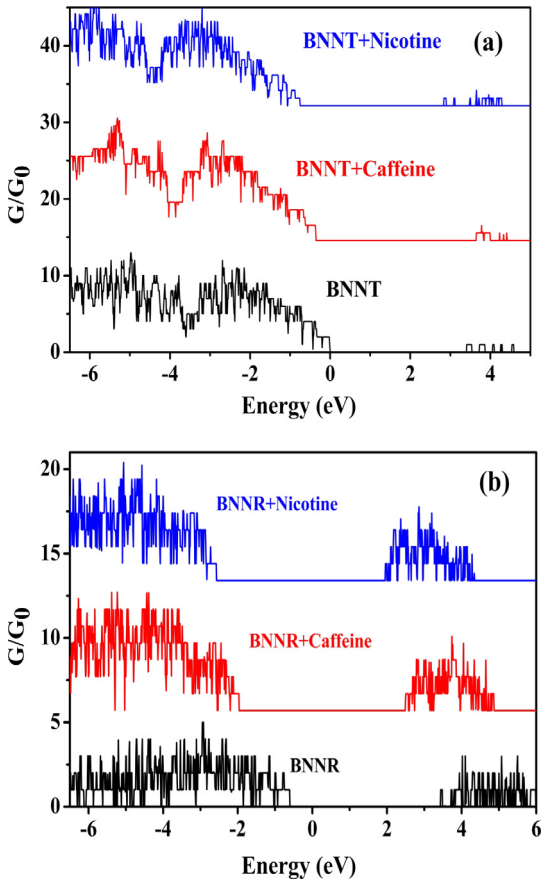

Fig. 8. Quantum conductance plot of (a) conjugated BNNT with Nicotine and Caffeine; (b) conjugated BNNR with Nicotine and Caffeine.

4. Conclusion

The interaction mechanism of two alkaloids caffeine and nicotine molecules with BNNT and BNNR is studied for the application of sensing of molecules using first principles calculations within dispersion corrected density functional theory. A detailed and systematic investigation is performed to obtain the stable geometrical properties, adsorption energy, electronic structure, charge transfer and quantum conductance for two alkaloids. It is shown that the caffeine and nicotine molecules are strongly adsorbed over BNNR than BNNT. The binding strength of these molecules is found to be stronger with the incorporation of dispersion correction and hence reinforces that the dispersion correction is essential for an accurate description of the adsorption process. No noticeable charge transfer is observed between the molecules and BNNT/BNNR. The caffeine presents stronger physisorption with both nanostructure but more with BNNR as compared to nicotine. The change in the DOS is due to adsorption of charge donor molecules. More sensitivity of the electronic properties of BNNR in the presence of caffeine and nicotine indicates that the BNNR as promising nanostructures for detection of these molecules. The present study emphasizes that the BNNR is an effective substrate to non-covalently binding alkaloid molecules. The reliable conclusions drawn in this study will encourage experimentalists to explore and use these nanostructures as alkaloid carriers, filters and sensors.

Acknowledgment

The study is financially supported by a research project from Science and Engineering Research Board (SERB) (SR/S2/CMP-

0005/2013), Govt. of India. SDD is thankful to the Department of Science and Technology, India for the INSPIRE senior research fellowship. The computations are carried out using high performance computer cluster provided under DST-FIST program.

References

[1] Y.F. Zhukovskii, S. Piskunov, J. Kazerovskis, D.V. Makaev, Comparative theoretical analysis of BN nanotubes doped with Al, P, Ga, As, In, and Sb, J. Phys. Chem. C 117 (2013) 14235–14240, https://doi.org/10.1021/jp3122903.

[2] N.G. Chopra, R.J. Luyken, K. Cherrey, V.H. Crespi, M.L. Cohen, S.G. Louie, A. Zettl, Boron nitride nanotubes, Science 269 (1995) 966–967, https://doi.org/10.1126/science.269.5226.966.

[3] X. Fua, R. Zhang, Energetics of hexagonal boron nitride nanostructures: edge dependence and truncation effects, Nanoscale 9 (2017) 6734–6740, https://doi.org/10.1039/C7NR00933J.

[4] Y. Chen, J. Zou, S.J. Campbell, G. Le Caer, S.J. Campbell, G.L. Caer, Boron nitride nanotubes: pronounced resistance to oxidation, Appl. Phys. Lett. 84 (2004) 2430–2432, https://doi.org/10.1063/1.1667278.

[5] S. Kalay, Z. Yilmaz, O. Sen, M. Emanet, E. Kazanc, Synthesis of boron nitride nanotubes and their applications, Beilstein J. Nanotechnol. 6 (2015) 84–102, https://doi.org/10.3762/bjnano.6.9.

[6] S.D. Dabhi, P.K. Jha, Dynamical properties of ultrathin armchair boron nitride nanotubes using density functional theory, Mater. Res. Express 3 (2016) 085015–085021, https://doi.org/10.1088/2053-1591/3/8/085015.

[7] S. Trivedi, S. Kumar, S.C. Sharma, S.P. Harsha, Biosensing application of multiwall boron nitride nanotube-based nanoresonator for detecting various viruses, IET Nanobiotechnol. 9 (2015) 259–263, https://doi.org/10.1049/iet-nbt.2014.0048.

[8] B. Aksoy, A. Paşahan, Ö. Güngör, S. Köytepe, A novel electrochemical biosensor based on polyimide-boron nitride composite membranes, Int. J. Polym. Mater. Polym. Biomater. 66 (2017) 203–212, https://doi.org/10.1080/00914037.2016.1201763.

[9] G. Ciofani, Potential applications of boron nitride nanotubes as drug delivery systems, Expert Opin Drug Deliv. 7 (2010) 889–893, https://doi.org/10.1517/17425247.2010.499897.

[10] G. Ciofani, V. Mattoli, Boron Nitride Nanotubes in Nanomedicine, first ed., Elsevier Science & Technology Books, Netherlands, 2016.

[11] D. Golberg, Y. Bando, Y. Huang, T. Terao, M. Mitome, C. Tang, Boron nitride nanotubes and nanosheets, ACS Nano 4 (2010) 2979–2993, https://doi.org/10.1021/nn1006495.

[12] A. Pakdel, C. Zhi, Y. Bando, D. Golberg, Low-dimensional boron nitride nanomaterials, Mater. Today. 15 (2012) 256–265, https://doi.org/10.1016/S1369-7021(12)70116-5.

[13] X. Chen, P. Wu, M. Rousseas, D. Okawa, Z. Gartner, A. Zettl, Boron nitride nanotubes are noncytotoxic and can be functionalized for interaction with proteins and cells, J. Am. Chem. Soc. 131 (2009) 890–891, https://doi.org/10.1021/ja807334b.

[14] Z. Zhang, W. Guo, Energy-gap modulation of BN ribbons by transverse electric fields: first-principles calculations, Phys. Rev. B 77 (2008) 075403–075408, https://doi.org/10.1103/PhysRevB.77.075403.

[15] Y. Zhang, X. Wu, Q. Li, J. Yang, Linear band-gap modulation of graphane nanoribbons under uniaxial elastic strain: a density functional theory study, J. Phys. Chem. C 116 (2012) 9356–9359, https://doi.org/10.1021/jp301691z.

[16] R.B. Chen, C.P. Chang, F.L. Shyu, M.F. Lin, Optical excitations of boron nitride ribbons and nanotubes, Solid State Commun. 123 (2002) 365–369, https://doi.org/10.1016/S0038-1098(02), 00295-8.

[17] K. Zhao, M. Zhao, Z. Wang, Y. Fan, Tight-binding model for the electronic structures of SiC and BN nanoribbons, Phys. E. 43 (2010) 440–445, https://doi.org/10.1016/j.physe.2010.08.025.

[18] R.M. Ribeiro, N.M.R. Peres, Stability of boron nitride bilayers: ground-state energies, interlayer distances, and tight-binding description, Phys. Rev. B 83 (2011) 235312–235317, https://doi.org/10.1103/PhysRevB.83.235312.

[19] J. Nakamura, T. Nitta, A. Natori, Electronic and magnetic properties of BNC ribbons, Phys. Rev. B 72 (2005) 205429–205433, https://doi.org/10.1103/PhysRevB.72.205429.

[20] A.J. Du, S.C. Smith, G.Q. Lu, First-principle studies of electronic structure and C-doping effect in boron nitride nanoribbon, Chem. Phys. Lett. 447 (2007) 181–186, https://doi.org/10.1016/j.cplett.2007.09.038.

[21] C.K. Yang, Exploring the interaction between the boron nitride nanotube and biological molecules, Comput. Phys. Commun. 182 (2011) 39–42, https://doi.org/10.1016/j.cpc.2010.07.040.

[22] D. Farmanzadeh, S. Ghazanfary, Interaction of vitamins A, B1, C, B3 and D with zigzag and armchair boron nitride nanotubes: a DFT study, Comptes Rendus - Chim. 17 (2014) 985–993, https://doi.org/10.1016/j.crci.2013.11.012.

[23] E.C. Anota, Y. Tlapale, M.S. Villanueva, J.A.R. Márquez, Non-covalent functionalization of hexagonal boron nitride nanosheets with guanine, J. Mol. Model. 21 (2015) 215–220, https://doi.org/10.1007/s00894-015-2768-0.

[24] B. Cai, S. Zhang, Z. Yan, H. Zeng, Noncovalent molecular doping of two-dimensional materials, ChemNanoMat 1 (2015) 542–557, https://doi.org/10.1002/cnma.201500102.

[25] Q. Weng, B. Wang, X. Wang, N. Hanagata, X. Li, D. Liu, X. Wang, X. Jiang, Y. Bando, D. Golberg, Highly water-soluble, porous, and biocompatible boron nitrides for anticancer drug delivery, ACS Nano 8 (2014) 6123–6130, https://doi.org/10.1021/nn5014808.

[26] I.V. Sukhorukova, I.Y. Zhitnyak, A.M. Kovalskii, A.T. Matveev, O.I. Lebedev, X. Li, N.A. Gloushankova, D. Golberg, D.V. Shtansky, Boron nitride nanoparticles with a petal-like surface as anticancer drug-delivery systems, ACS Appl. Mater. Interf. 7 (2015) 17217–17225, https://doi.org/10.1021/acsami.5b04101.

[27] S.M. Chowdhury, G. Lalwani, K. Zheng, J.Y. Yang, K. Neville, B. Sitharaman, Cell specific cytotoxicity and uptake of graphene nanoribbons, Biomaterials 34 (2013) 283–293, https://doi.org/10.1016/j.biomaterials.2012.09.057.

[28] H. Zhang, G. Gruner, Y. Zhao, Recent advancements of graphene in biomedicine, J. Mater. Chem. B 1 (2013) 2542–2567, https://doi.org/10.1039/C3TB20405G.

[29] J. Rusted, L. Graupner, N. O'Connell, C. Nicholls, Does nicotine improve cognitive function?, Psychopharmacology 115 (1994) 547–549, https://doiorg/10.1007/BF02245580.

[30] D. Bishop, Dietary supplements and team-sport performance, Sports Med. 40 (2010) 995–1017, https://doi.org/10.2165/11536870-000000000-00000.

[31] D. Robertson, D. Wade, R. Workman, R. Woosley, J.A. Oates, Tolerance to the humoral and hemodynamic effects of caffeine in man, J. Clin Invest. 67 (1981) 1111–1117, https://doi.org/10.1172/JCI110124.

[32] Z.G. Chen, L.S. Zhang, Y.W. Tang, Z.J. Jia, Adsorption of nicotine and tar from the mainstream smoke of cigarettes by oxidized carbon nanotubes, Appl. Surf. Sci. 252 (2006) 2933–2937, https://doi.org/10.1016/j.apsusc.2005.04.044.

[33] E.C. Girão, S.B. Fagan, I. Zanella, A.G. Souza, Nicotine adsorption on single wall carbon nanotubes, J. Hazard. Mater. 184 (2010) 678–683, https://doi.org/10.1016/j.jhazmat.2010.08.091.

[34] H.J. Lee, G. Kim, Y.K. Kwon, Molecular adsorption study of nicotine and caffeine on single-walled carbon nanotubes from first principles, Chem. Phys. Lett. 580 (2013) 57–61, https://doi.org/10.1016/j.cplett.2013.06.033.

[35] J. Wang, V.K. Kayastha, Y.K. Yap, Z. Fan, J.G. Lu, Z. Pan, I.N. Ivanov, A.A. Puretzky, D.B. Geohegan, Low temperature growth of boron nitride nanotubes on substrates, NanoLett. 5 (2005) 2528–2532, https://doi.org/10.1021/nl051859n.

[36] L.H. Li, J. Cervenka, K. Watanabe, T. Taniguchi, Y. Chen, Strong oxidation resistance of atomically thin boron nitride nanosheets, ACS Nano 8 (2014) 1457–1462, https://doi.org/10.1021/nn500059s.

[37] C.Y. Zhi, Y. Bando, C.C. Tang, Q. Huang, D. Golberg, Boron nitride nanotubes: functionalization and composites, J. Mater. Chem. 18 (2008) 3900–3908, https://doi.org/10.1039/b804575e.

[38] A. Soltani, M.T. Baei, E.T. Lemeski, M. Shahini, Superlattices and microstructures sensitivity of BN nano-cages to caffeine and nicotine molecules, Superlattic. Microstruct. 76 (2014) 315–325, https://doi.org/10.1016/j.spmi.2014.09.031.

[39] M.T. Baei, B 12 N 12 sodalite like cage as potential sensor for hydrogen cyanide, Comput. Theor. Chem. 1024 (2013) 28–33, https://doi.org/10.1016/j.comptc.2013.09.018.

[40] M.D. Esrafili, R. Nurazar, A density functional theory study on the adsorption and decomposition of methanol on B 12 N 12 fullerene-like nanocage, Superlattic. Microstruct. 67 (2014) 54–60, https://doi.org/10.1016/j.spmi.2013.12.020.

[41] S. Mukhopadhyay, R.H. Scheicher, R. Pandey, S.P. Karna, Sensitivity of boron nitride nanotubes toward biomolecules of different polarities, J. Phys. Chem. Lett. 2 (2011) 2442–2447, https://doi.org/10.1021/jz2010557.

[42] X. Zhong, S. Mukhopadhyay, S. Gowtham, R. Pandey, S.P. Karna, Applicability of carbon and boron nitride nanotubes as biosensors: effect of biomolecular adsorption on the transport properties of carbon and boron nitride nanotubes, Appl. Phys. Lett. 102 (2013) 133705–133708, https://doi.org/10.1063/1.4801442.

[43] J.P. Perdew, K. Burke, M. Ernzerhof, generalized gradient approximation made simple, Phys. Rev. Lett. 77 (1996) 3865–3868, https://doi.org/10.1103/PhysRevLett. 77.3865.

[44] P. Giannozzi et al., QUANTUM ESPRESSO: a modular and open- source software project for quantum simulations of materials, J. Phys. Condens. Matter. 21 (2009) 395502–395520, https://doi.org/10.1088/0953-8984/21/39/395502.

[45] H.J. Monkhorst, J.D. Pack, Special points for Brillouin-zone integrations, Phys. Rev. B 13 (1976) 5188–5192, https://doi.org/10.1103/PhysRevB.13.5188.

[46] B. Civalleri, L. Maschio, P. Ugliengo, C.M.Z. Wilson, Role of dispersive interactions in the CO adsorption on MgO(0 0 1): periodic B3LYP calculations augmented with an empirical dispersion term, PCCP 12 (2010) 6382–6386, https://doi.org/10.1039/c002146f.

[47] S. Grimme, Semiempirical GGA-type density functional constructed with a long-range dispersion correction, J. Comput. Chem. 27 (2006) 1787–1799, https://doi.org/10.1002/jcc.

[48] R. Landauer, Electrical resistance of disordered one- dimensional lattices, Phil. Mag. 21 (2016) 863–867, https://doi.org/10.1080/14786437008238472.

[49] A.A. Mostofi, J.R. Yates, Y. Lee, I. Souza, D. Vanderbilt, N. Marzari, wannier90: a tool for obtaining maximally-localised Wannier functions, Comput. Phys. Commun. 178 (2008) 685–699, https://doi.org/10.1016/j.cpc.2007.11.016.

[50] O. Kwon, M.L. Mckee, Theoretical calculations of band gaps in the aromatic structures of polythieno [3,4-b] benzene and polythieno [3,4-b] pyrazine, J. Phys. Chem. A 104 (2000) 7106–7112, https://doi.org/10.1021/jp000434g.

[51] H. Yildirim, T. Greber, A. Kara, Trends in adsorption characteristics of benzene transition metal surfaces: role of surface chemistry and Van Der Waals interactions, J. Phys. Chem. C 117 (2013) 20572–20583, https://doi.org/10.1021/jp404487z.

[52] L. Debbichi, Y.J. Dappe, M. Alouani, Effect of van der Waals interaction on energetics and transport properties of a single anthracene molecule adsorbed

or confined inside a carbon nanotube, Phys. Rev. B 85 (2012) 045437–045442, https://doi.org/10.1103/PhysRevB.85.045437.
[53] S. Mukhopadhyay, S. Gowtham, R.H. Scheicher, Theoretical study of physisorption of nucleobases on boron nitride nanotubes: a new class of hybrid nano-biomaterials, Nanotechnology. 21 (2010) 165703–165709, https://doi.org/10.1088/0957-4484/21/16/165703.
[54] R. Tadmor, The London – van der Waals interaction energy between objects of various geometries, J. Phys. Condens. Matter. 13 (2001) 195–202, https://doi.org/10.1088/0953-8984/13/9/101.
[55] A. Calvi, A. Ferrari, L. Sbuelz, A. Goldoni, S. Modesti, Recognizing physisorption and chemisorption in carbon nanotubes gas sensors by double exponential fitting of the response, Sensors 16 (2016) 731–739, https://doi.org/10.3390/s16050731.
[56] T. Fujimori, A.M. Gomez, Z. Zhu, H. Muramatsu, R. Futamura, K. Urita, M. Terrones, T. Hayashi, M. Endo, S.Y. Hong, Y.C. Choi, D. Toma, K. Kaneko, Conducting linear chains of sulphur inside carbon nanotubes, Nat. Commun. 4 (2013) 2162–2169, https://doi.org/10.1038/ncomms3162.

Journal of Materials Chemistry B

PAPER

Cite this: J. Mater. Chem. B, 2018, 6, 6796

"Haeckelite", a new low dimensional cousin of boron nitride for biosensing with ultra-fast recovery time: a first principles investigation†

Basant Roondhe and Prafulla K. Jha *

Received 22nd June 2018,
Accepted 25th September 2018

DOI: 10.1039/c8tb01649f

rsc.li/materials-b

We performed state-of-the-art first principles calculations under the framework of dispersion corrected density functional theory to investigate the electronic and vibrational properties of a recently found allotrope of BN, with octagonal and square ring forming planar haeckelite structures (haeck-BN). We further investigated the adsorption mechanism of five nucleobases adenine (A), guanine (G), cytosine (C), thymine (T) and uracil (U) over haeck-BN to explore its applicability in biosensing. The dispersion correction (DFT-D2) is included to appropriately consider van der Waals interactions. The order of adsorption energy of nucleobases over haeck-BN has the following order: G > T > A ≈ C > U. Significant variation in electronic properties, density of states and work function confirm the adsorption of nucleobases. To check the reusability of haeck-BN as a biosensor toward nucleobases, we calculated the recovery time. Ultrafast recovery times (in millisecond) of 292 ms, 130 ms, 120 ms, 160 ms and 0.6 ms were predicted for G, A, C, T and U, respectively. Our finding suggests that haeck-BN can be utilized as a biosensor for the detection of nucleobases due to its superiority to graphene, h-BN and boron nitride nanotubes, and can be further explored for photocatalysis.

1. Introduction

The last decades were extensively dedicated to the study of a wide range of carbon-based materials. Due to the remarkable properties of new carbon forms, such as fullerenes, carbon nanotubes and graphene, considerable interest has been developed among the scientific community for their use in several technological areas.[1–4] Among all carbon forms, graphene has attracted considerable research interest since its successful fabrication in 2004.[4] Graphene has a symmetrical hexagonal honeycomb atomic structure, resulting in its extraordinary and excellent physical properties.[5–10] Through extensive investigation of this outstanding material, it has been demonstrated as a promising material for spin and nanoelectronics.[11,12] The discovery of graphene, which confirmed the existence of 2D materials, motivated the researchers to explore other 2D materials. Thus so far, monolayers of h-boron nitride (h-BN), silicon, transition metal sulfides, phosphorous and many other materials have been synthesized or predicted.[13–21] A significant impact for the development of nanodevices and nanoelectronics has been demonstrated by these 2D materials due to their astonishing electrical, optical, and mechanical properties.[5–12] 2D materials, which have the typical hexagonal structure, have gathered attention because of the impact of such a structure on various properties of the material. This is because in any material, the properties are associated with the position of the atoms in the structure and can influence the formation of electronic structures in the materials. BN nanostructures, which are isomorphic to carbon, have been extensively explored for their immense chemical and thermal stability by virtue of their exceptional properties.[22,23] Owing to the geometrical similarity, h-BN sheet, which is an insulator with large bandgap in contrast to the semimetal graphene, possesses many excellent properties similar to graphene, such as good thermal conductivity, strong mechanical properties and high thermal stability.[24,25] Graphene has non-polar C-C bonding, whereas B–N bond is highly polar in h-BN sheet.[26,27] Due to these unique properties, h-BN sheets have found applications in lubricants, dielectric materials, as insulators in electronic devices, *etc.*[28,29]

The existence of new structures in 2D materials was demonstrated by the presence of the square-octagonal pair in BN monolayer grown on Cu(111) surface[30] as defect states of h-BN. This formation of square-octagonal pair in h-BN was also predicted by Liu *et al.*[31] Following these studies, periodic structures consisting square-octagonal pairs of GaN[32] and ZnO[33] were theoretically predicted and studied. However, the possibility of

Department of Physics, Faculty of Science, The Maharaja Sayajirao University of Baroda, Vadodara-390002, India. E-mail: prafullaj@yahoo.com, pk.jha-phy@msubaroda.ac.in

† Electronic supplementary information (ESI) available: Charge density plots, HOMO–LUMO, partial density of states (PDOS) and work function plots of nucleobases adsorbed haeck-BN system. See DOI: 10.1039/c8tb01649f

similar periodic structures with repeating square-octagonal pairs of boron and nitrogen was not yet considered to the best of our knowledge, even though the existence of square-octagonal units in h-BN were proven experimentally. Thus, motivated by the experimental work of Li *et al.* and the theoretical studies of haeckelite GaN and ZnO, we performed the first principles calculations of haeck-BN.

Deoxyribonucleic acid (DNA) and Ribonucleic acid (RNA) have been the main focus of researchers from the past few decades as they are the key components of genome and the centre of biological systems. The basic building blocks of nucleotides are nucleobases that carry all the information of DNA, with purine as its base compound. Many studies have been reported that provide a brief description of sensing phenomena of nanostructures with nucleobases.[34–40] There are few advantages of h-BN over graphene, such as lower hydrophobicity (which minimizes its hydrophobic interaction with DNA to avoid its translocation), lower thickness compared with the nucleotide spacing in single stranded DNA[41] and unchanged fundamental properties of both h-BN and DNA, which are important for DNA research.[42] Zhi *et al.*[36] have reported stronger interactions between BN nanostructures and nucleobases compared with graphene due to the presence of dissimilar atoms. The cytocompatibility of boron nitride nanostructure (BNNs) with living cell has also been reported.[37,38] Liu *et al.*[39] and Zhang and Wang[40] have reported genome and DNA sequencing using BN nanopores. Jin *et al.*[43] explored MoS_2 as a biosensor and reported improvement in the sensing of nucleobases by modifying its surface with Au. All these studies have enhanced our understanding about the utilization of BNNs in nano-biomedical applications.[44,45]

Motivated with the success of BNNs in sensing and detecting biomolecules, we explored this new haeck-BNNs, *i.e.*, haeckelite boron nitride nanostructure, as a possible biosensor. Due to the different interatomic distances and bond angles in two dimensional haeckelite structures compared with other usual two dimensional structures arising due to an octagonal and square ring structure, these haeckelite structures are expected to interact differently with the adsorbates similar to the porous material. Furthermore, a different type of interaction between adsorbate and haeck-BN is foreseen because of the presence of all the atoms present in haeck-BN unit cells. To the best of our knowledge, 2D haeckelite monolayer structure of BN has not been explored theoretically for biosensing applications. In the present study, we aim to investigate the structural, electronic and phonon properties of haeck-BN. While electronic properties of haeck-BN show the possibility of its use in electronic devices, the phonon properties will be of use in understanding its thermal properties apart from its prominent dynamical stability. Finally, we studied the adsorption mechanism of nucleobases over its surface. The study of structural geometries, electronic properties, phonon dispersion of haeck-BN, adsorption and charge transfer of haeck-BN functionalized by adenine (A), thymine (T), guanine (G), cytosine (C) and uracil (U) nucleobases was conducted. State-of-the-art *ab initio* calculations were performed to uncover the dispersion effect on the interaction of nucleobases with haeck-BN. Thus, in this study, we reveal the nature of interaction of nucleobases with haeck-BN to obtain an atomic level understanding about these hybrid systems for various applications.[46,47]

The paper is organized as follows. The computational details are given in Section 2. Structural and electronic properties of the haeck-BN monolayer are described in Section 3.1. The phonon dispersion of haeck-BN monolayer is discussed in Section 3.2. The adsorption mechanisms are described in Section 3.3. Finally, the conclusion is provided in Section 4.

2. Computational methods

All calculations were performed using first principles calculation under the framework of density functional theory (DFT) implemented in Quantum Espresso code,[48] which uses plane-wave basis sets to expand the Kohn–Sham orbital. The Broyden–Fletcher–Goldfarb–Shanno (BFGS)[49] method was used for ground state optimization of all the structures. Generalized gradient approximation (GGA) proposed by Perdew–Burke–Ernzerhof (PBE) was employed to treat the exchange–correlation functional in ultrasoft pseudo potential.[50] The plane wave basis set with 80 Ry and 800 Ry cut off energy and charge density, respectively, was used for single particle functions, which were sufficient to fully converge the lattice parameters and total energy. Brillouin zone (BZ) integration was performed within the Monkhorst–Pack[51] scheme with k-mesh $16 \times 16 \times 1$ for the unit cell and $8 \times 4 \times 1$ for the (2×3) supercell (the convergence plots of kinetic energy cutoff and number of k-points are provided in ESI,† Fig. S1). These k-points mesh guarantee a violation of charge neutrality less than $0.009e$, indicating adequate convergence of the calculations. Iterative Davidson type diagonalization method was used to solve the Kohn–Sham equation with energy convergence threshold of 1×10^{-8} Ry. Density functional perturbation theory (DFPT) implemented in Quantum Espresso code[52] was used to compute the phonon properties, which allows the calculation of phonons at any wave vector in the unit cell. A q mesh of $10 \times 10 \times 1$ was used to calculate dynamical matrix for 2D monolayer of haeck-BN by applying acoustic sum rule for $q \rightarrow 0$. Dynamic stability was also ensured by the phonon frequencies calculation along the entire Brillouin Zone (BZ), which was computed by the forces obtained after the perturbation method in quantum espresso package. Comparative analysis was performed to understand the interaction of haeck-BN with five nucleobases by structural optimization, adsorption energy calculation and density of states (DOS) plots. Accounting of the dispersion forces has been emphasized in the literature by a precise quantum mechanical description that explains the interaction of a molecule with a nanosurface.[53] Therefore, for the description of long-range electron correlation, it is important to choose a suitable computational method. The present study employed Grimme's dispersion correction[54] to consider the long range van der Waals interaction (*i.e.* $\sim$3 Å) between the nucleobases and the haeck-BN monolayer.

The adsorption energy E_{ad} has been calculated according to the following equation:

$$E_{ad} = E_{(haeck\text{-}BN+necleobase)} - \{E_{(haeck\text{-}BN)} + E_{(nucleobase)}\} \quad (1)$$

where $E_{(haeck\text{-}BN+nucleobase)}$ is the total energy of haeck-BN adsorbed by nucleobase (adenine (A), thymine (T), guanine (G), cytosine (C) and uracil (U)), $E_{(haeck\text{-}BN)}$ is the total energy of the adsorbent haeck-BN monolayer, and $E_{(nucleobase)}$ is the total energy of the nucleobase (A, T, G, C and U) obtained from their fully optimized geometries.

3. Results and discussion

3.1 Structural and electronic properties

To understand the structural and electronic properties of any system, the system should be fully relaxed and optimized. We first optimized the geometry and related parameters of the primitive cell of the haeck-BN monolayer structure by calculating its lattice constant and ground state energy. The optimized structure of the haeck-BN monolayer is shown in Fig. 1(a). From the figure, it is clear that the primitive cell, which has tetragonal $P4/mbm$ (127) space group, is different from bulk h-BN as well as from 2D h-BN, as shown in Fig. 1(b and c). While bulk BN has $P6_3/mmc$ (194), $P6_3mc$ (186) and $F4\bar{3}m$ (216) space groups for bulk h-BN, wurtzite BN and zinc blende BN,[55,56] respectively, 2D h-BN has hexagonal honeycomb lattice with $P\bar{6}2m$ (189) space group. The haeck-BN unit cell has an entire atom situated at the center but not at the corner. The haeck-BN structure has octagonal and square rings, which give different interatomic distances and bond angles. The bond distance d of B–N is 1.402 Å in square ring and 1.475 Å in octagonal ring. The calculated bond angles in the square ring are 84.21° and 95.78°, while in the octagonal ring, the bond angles are 132.10° and 137.11°. The bond length of B–N in haeck-BN monolayer is significantly different from the bulk BN as well as 2D h-BN as the bond length between B–N varies from 1.45 to 1.568 Å.[55] The bond length of B–N in haeck-BN is 0.045 Å less in square ring as compared with that in h-BN, while the bond length between B–N at octagonal ring is larger by 0.025 Å. This is the major structural difference between the two monolayers h-BN and haeck-BN. The optimized lattice parameter along with calculated bond angles and bond length are presented in Table 1.

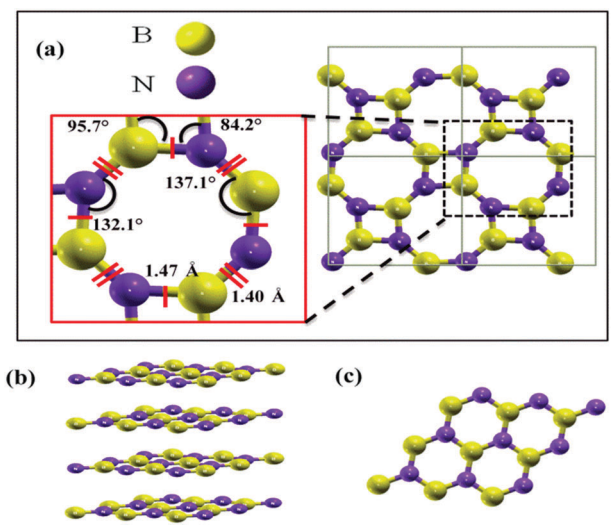

Fig. 1 (a) Optimized structure of haeck-BN monolayer and enlarged view having bond lengths and bond angles, (b and c) structure of bulk h-BN and 2D h-BN. Yellow and purple balls represents boron and nitrogen, respectively.

As known that the electronic band structure is key to understanding the electronic properties of any material, we further calculated the band structure of haeck-BN. An important information about the mass of the electron can also be found from the band dispersion. The calculated band structure for haeck-BN along k path Γ–M–X–Γ of the Brillouin Zone (BZ) is shown in Fig. 2, along with the density of states and orbital contribution as PDOS. Highly dispersive bands in the conduction band region suggest small effective mass for electron. A direct band gap of 3.9 eV is observed between Γ–M, which is lower than that of bulk h-BN, z-BN and w-BN, which have large indirect band gap of 4.47 eV, 5.72 eV and 4.50 eV respectively.[55] The significantly lower and direct bandgap in haeck-BN makes it an interesting material to be explored for optoelectronics and biosensors.[57] Boron and nitrogen atoms contribute equally to form the electronic band structure of haeck-BN. The right panel of Fig. 2 presents the total and partial density of states of haeck-BN for proper understanding of the electronic contribution. From the figure, we can see that the boron atoms have a dominating contribution in the conduction band (between 2–6 eV) with its p_x orbitals, while p_y and p_z have minor contributions in the valence band (between −4 to −8 eV). The nitrogen atom contributed majorly in the valence band region with its p_x orbital electron between −2 to −4 eV, while p_y and p_z contributed in the lower valence band region between −4 to −8 eV. However, in case of bulk BN, the valence band maxima mainly comprises of N-p_z and the conduction band has contributions from the B-p_z orbitals.[55]

In order to predict the chemical bonding and the charge transfer in haeck-BN, the charge-density behaviors were calculated in the (110) plane for this compound and are depicted in Fig. 3. Electronegativity values for B and N are +0.1196 and +0.4657, respectively. The plot shows covalent bonding between B and N atoms in haeck-BN. The iso-density plot shows no vacancy as density is evenly distributed throughout. The charge between B and N is shared by the covalent bond between them. The maximum charge accumulation sight is near nitrogen atom (blue color; +0.4657), which shows the localization of electron around it.

3.2 Vibrational properties

Phonon dispersion calculations are crucial in understanding the dynamical stability of any materials, as it provides an insight into the mechanical, acoustic, spectroscopic, thermodynamic and dynamical properties at finite temperatures. Diagonalization of dynamic matrix was used to calculate the phonon dispersion curves (PDC), which provides insight on the stability, as it is a reliable test that checks the dynamical stability. The calculated

Table 1 Calculated lattice a (Å), bond length (Å), bond angle (°), energy band gap E_g (eV), and Fermi level energies E_F (eV) of haeck-BN

System	Lattice a (Å)	Bond angle (°)	Bond length (Å)	E_F (eV)	E_g (eV)
Haeck-BN	4.929	84.21 and 95.78 (for square ring) 132.10 and 137.11 (for octagonal ring)	1.402 (bond in square ring) 1.475 (bond in octagonal ring)	−2.332	3.91

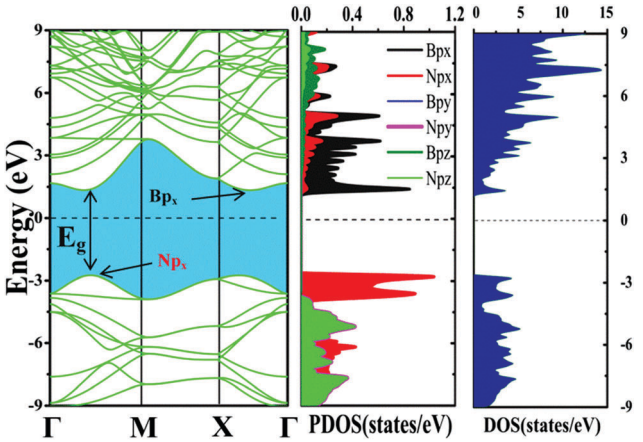

Fig. 2 Calculated band dispersion curve of haeck-BN, along with total DOS and PDOS of haeck-BN (right panel).

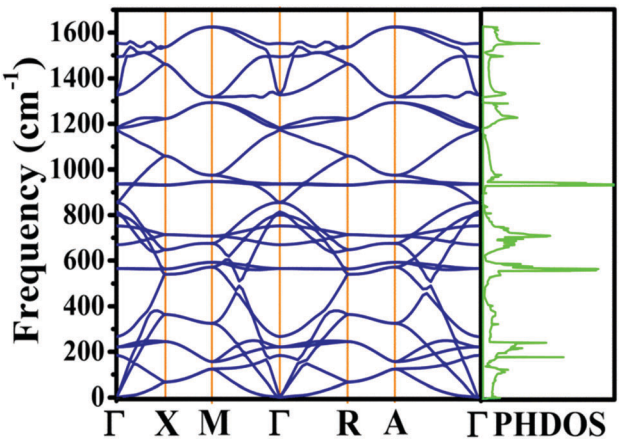

Fig. 4 Phonon dispersion curve along with the phonon density of states (PHDOS).

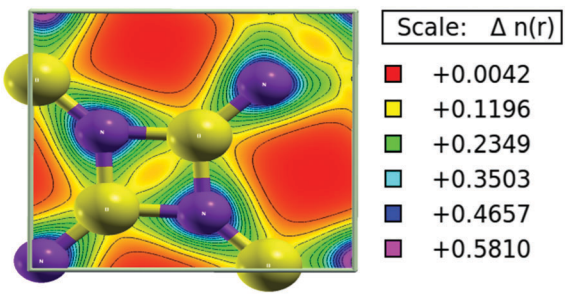

Fig. 3 Total charge density plot of haeck-BN. Blue colour represents larger value of electron charge density while red colour shows relatively low charge density.

PDC for haeck-BN along with the phonon density of states (PHDOS) are presented in Fig. 4. The number of branches in the dispersion curve depends upon the number of atoms in the unit cell. Presence of N atoms in the unit cell, results into 3N phonon branches, with 3 acoustical and 3N–3 optical modes.[53] There are eight atoms in the unit cell of haeck-BN, for which there are 24 phonon branches, whereas in 2D h-BN, two atoms per unit cell result in six phonon branches.[55,58,59] Each mode is labeled according to its polarization, and the letters 'L', 'T' and 'Z' stand for longitudinal, transverse and out-of-plane vibrations, respectively. Letters 'A' and 'O' represent the acoustic and optical modes, respectively. The longitudinal acoustic (LA) and transverse acoustic (TA) modes show linear dispersion around the Γ point, while the out of plane acoustic (ZA) mode exhibits quadratic dispersion, which is characteristic of 2D layered materials.[21,59,60] This quadratic behavior of the ZA band, which arises due to D_{6h} point group symmetry, can be attributed to the fact that at the lowest-order amplitude, strain energy, which is induced by this vibration, is altogether associated with the arching of this out-of-plane bending mode induced in the monolayer.[61]

The PDC plotted in high symmetry directions of the Brillouin Zone (BZ) does not have any phonon modes with imaginary frequency throughout BZ, indicating dynamical stability of haeck-BN similar to other haeckelite compounds.[32,33] The quadratic ZA mode is closely associated with bending rigidity and lattice heat capacity of the nanosheet in the long-wavelength (small $\bar{q}$) region. Moreover, softening of the transverse acoustic (TA) and longitudinal acoustic (LA) modes is observed, indicating reduced group velocities. It is noteworthy that these reduced group velocities can be of use in improving the thermoelectric figure of merit ZT as it reduces thermal conductivity.[62] The ZA mode, which behaves greatly differently from TA and LA modes, will have even lower group velocity due to a parabolic dispersion near the Γ point. There is no gap observed in between acoustic and optical branches due to the low mass difference between boron and nitrogen atoms, similar to h-BN.[59] The phonons of the haeck-BN sheet show considerable softening compared with those of the h-BN sheet, which can be attributed to the fact that the elastic constants of haeck-BN may be smaller than those of h-BN. In PDC of haeck-BN, at Γ point, we observed nine singly (A) and six doubly (E) degenerated optical phonon modes, *i.e.*, $\Gamma = 9A + 6E$. All 24 modes in haeck-BN are equally distributed in frequencies ranging from 0 to ~1600 cm^{-1}. The stability was further confirmed by calculating the PHDOS, as shown in the right panel of Fig. 4. The phonon density of states is an important dynamical property as its computation requires phonon frequencies in the entire Brillouin zone and can be defined as[63]

$$g(\omega) = \frac{1}{N}\int_{BZ}\sum_{j}\delta\left[\omega - \omega_j(\bar{q})\right]d\bar{q} \qquad (2)$$

where N is the normalization constant such that $\int g(\omega)\mathrm{d}\omega = 1$. $g(\omega)\mathrm{d}\omega$ is the ratio of number of eigenstates in the frequency interval $(\omega, \omega + \mathrm{d}\omega)$ to the total number of eigenstates. $\omega_j(\vec{q})$ is the phonon frequency of jth phonon modes. The PHDOS calculation is a real test that helps us calculate not only lattice specific heat but also other thermodynamic functions in the entire BZ.[64,65] The ionic bonding between the sp^2 hybridized B and N atoms in haeck-BN is predominant in the high-frequency modes, which is quite similar to the phonon modes in previously reported sp^2 hybrid boron nitride structures.[59,66]

In the lower frequency region, the modes show dispersive behavior. This convergence can be attributed to the close sharing of potential energy in various modes. Since the dispersion of modes depends on the strength of interaction, a mixing character of modes due to repulsion gives different variations. Whole phonon modes from Γ–X come close and retain the same nature from X–M but split from M–Γ direction of BZ. The intense peaks at $\sim$600 and 900 cm^{-1} are attributed to the flat bands in dispersion curves. The additional weak singularity in the low frequency region is due to some of the strongly dispersed acoustical and low frequency optical phonon modes.

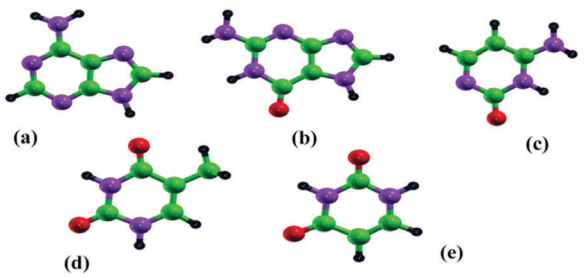

Fig. 5 Optimized structures of five nucleobases A, G, C, T and U. Red, green, black and purple balls correspond to oxygen, carbon, hydrogen and nitrogen atoms, respectively.

3.3 Adsorption mechanisms

To understand the mechanism of the interactions between haeck-BN and nucleobases, we first constructed a supercell (2×3) of haeck-BN with 48 atoms (24 B and 24 N atoms) to provide a large surface for nucleobases to interact. The full structural optimization of haeck-BN sheet and all considered nucleobases, *i.e.*, adenine (A), thymine (T), guanine (G), cytosine (C) and uracil (U), was conducted individually. The optimized structure of nucleobases adenine, thymine, guanine, cytosine and uracil are presented in Fig. 5(a–e).

Fig. 6(a–f) show the optimized geometries of pristine haeck-BN sheet and nucleobase-adsorbed haeck-BN sheet. We chose parallel orientation for all nucleobases over haeck-BN as previous works suggest the parallel position of the nucleobases over BN nanostructures due to its most stable configuration.[67,68] Our calculations of structural relaxation was initially started by placing the molecule near the surface of haeck-BN, and followed by full structural relaxation to obtain the ground state geometrical configuration. In the energetically stable configurations of all the considered systems, the adsorbed molecules attained a distance in the range of 2.5–2.9 Å from haeck-BN. This large distance of molecules from the haeck-BN monolayer prevents the formation of chemical bonds, leading to physisorption of the adsorbed molecules. Furthermore, to confirm the nature of absorption and distance of nucleobases from haeck-BN, we performed total energy calculations of each system, with molecules at distances varying in the range of 1–4 Å from haeck-BN. We found that the minimum energy configuration is obtained when all adsorbed molecules are placed at a distance of 2.5–2.9 Å from haeck-BN surface, which supports

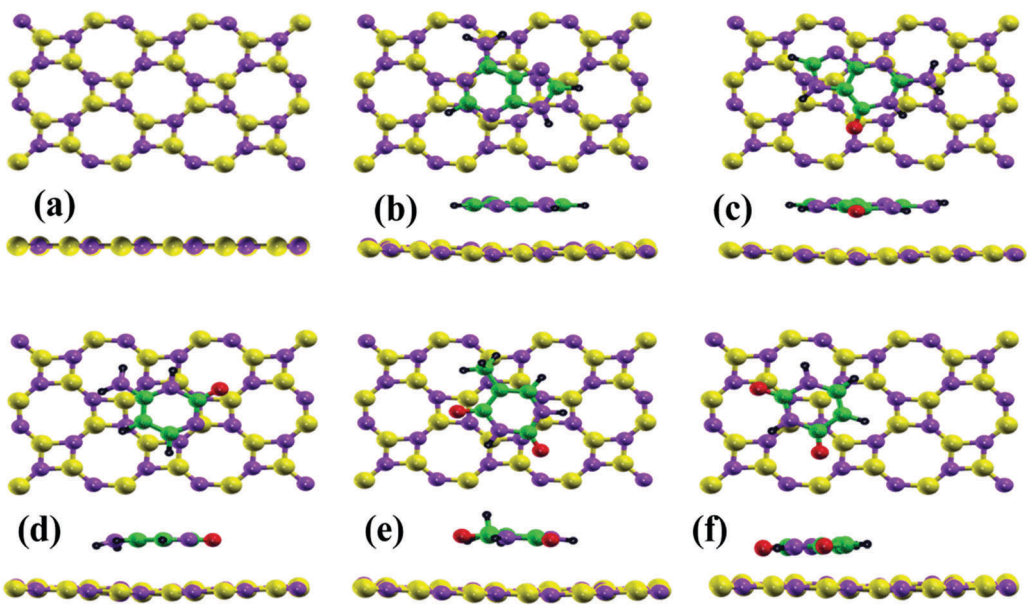

Fig. 6 Optimized structures of (a) pristine haeck-BN and nucleobases adsorbed haeck-BN for (b) adenine (c) guanine (d) cytosine (e) thymine and (f) uracil (top and side view).

our full structural relaxation calculations. We have also considered various orientations of nucleobases for better clarification, and tabulated the total energies of these configurations at different distances and orientations in Tables S1 and S2 of ESI.† The nature of adsorption is physical (physisorption) as the distance between nucleobases and haeck-BN sheet is large, *i.e.*, ~2.8 Å (as can be seen in Table 1). This large distance between nucleobases and haeck-BN sheet ensures the elimination of the possibility of any covalent bond formation. Long range van der Waals interactions were taken into account with the incorporation of dispersion correction in the present DFT (DFT-D2) calculations, as it increases binding/adsorption by about 8 to 10 times the normal PBE calculation.[69] We have not used new D3[70] correction as both D2 and D3 provide similar results in case of non-covalent interactions.[71] The adsorption energy (E_{ad}) calculated for A, G, C, T and U over haeck-BN are −0.662 eV, −0.742 eV, −0.660 eV, −0.668 eV and −0.525 eV, respectively, with binding distances (d) between 2.7 Å to 2.9 Å. Our adsorption energy results are better than the previously reported values of adsorption energy for h-BN as well as for graphene,[42,72–74] which can be attributed to the unique structural and electronic properties of haeck-BN. However, the sequence of adsorption of the nucleobases over haeck-BN (G > T > A ≈ C > U) is similar to the adsorption trend of nucleobases with other BN and carbon nanostructures.[42,72–74] Comparative results regarding adsorption energy of all five nucleobases on different nanomaterials are shown in Fig. 7. The van der Waals forces together with the stacking of the molecules on the surface are the reasons behind this difference in the adsorption energy.[75,76] The π–π stacking configuration has higher adsorption energy as it minimizes the repulsion due to π-orbital overlapping to prevent the molecules to get repelled from the nanosurface. This leads to the superior adsorption energy on nanosurface.[44,45]

The present results depict that the nucleobases are more effectively adsorbed on hacek-BN compared with graphene,[73,74] and other boron nitride nanostructures, such as h-BN,[42] BNNR[68] and BNNT.[77] The adsorption of molecules over haeck-BN sheet alters the electronic properties, which were inspected by calculating the band dispersion, band gap, density of states (DOS) and partial DOS (PDOS). The band dispersion curves of pristine and nucleobases-adsorbed haeck-BN sheet are presented in Fig. 8. A significant change in the band structure as well as band gap can be seen from the band dispersion. There are some impurity states generated within the band structure of pristine haeck-BN after the adsorption of nucleobases, which is mainly due to the p-orbital electrons of C, O and N atoms and a partial contribution from the s orbital of H atoms present in the nucleobases. Appearance of peculiar flat bands in the conduction as well as valence band region in the band structure is also observed after the adsorption of nucleobases. This is an interesting feature that can be attributed to the quenching of kinetic energy of the electrons.[78] The band structure after the adsorption of adenine on the surface of haeck-BN is depicted in Fig. 8(b), which shows the appearance of impurity states as flat bands at the top of the valence band region after adenine adsorption. These flat bands are created due to the participation of p_x orbital electron of nitrogen and carbon atoms present in the adenine molecule. In the valence band region near −1.9 eV and −4 eV (due to p_x orbital of N) and in the conduction band region near 2 eV (due to p_x orbital of C), such flat bands are observed. Similar behavior of bands in the band dispersion is observed for all the other nucleobases. In all nucleobases other than adenine, oxygen atom also takes part in the formation of flat bands. In guanine (Fig. 8(c)), oxygen p_x orbital plays a key role in the valence band region near −3 eV. However, after the adsorption of cytosine on the haeck-BN surface, a large modulation in the band gap is observed (Fig. 8(d)). Many flat bands in the band structure are generated in valence as well as conduction bands. This is a similar modification in the bands after thymine adsorption. However, uracil creates fewer number of flat bands only in the conduction band, which can be attributed to its size and number of atoms available for participation in the formation of extra electronic states (Fig. 8(e and f)). The band gap of haeck-BN reduces from 3.913 eV to 3.199 eV, 2.999 eV, 2.869 eV, 3.309 eV and 3.340 eV after adsorption of nucleobases A, G, C, T and U, respectively. We further analyzed the electron transport by calculating the Lowdin charge transfer. The significant charge transfer between the nucleobase and haeck-BN in the adsorption process indicates that the interaction of nucleobase can lead to modifications in structural and electronic properties of haeck-BN. A significant charge transfer of 0.14e, 0.15e, 0.10e, 0.11e and 0.09e for A, G, C, T and U, respectively, may be the reason for the bandgap modulation. The charge transfer can also be understood by charge density and HOMO–LUMO calculations.

The effect of these molecules on the charge density of pristine haeck-BN is understood by charge density calculations as it helps to predict the chemical bonding and also the charge transfer behavior between haeck-BN and nucleobases. The calculated charge density contours are presented in Fig S3 of the ESI.†

The Highest Occupied Molecular Orbital (HOMO) and the Lowest Unoccupied Molecular Orbital (LUMO) are the

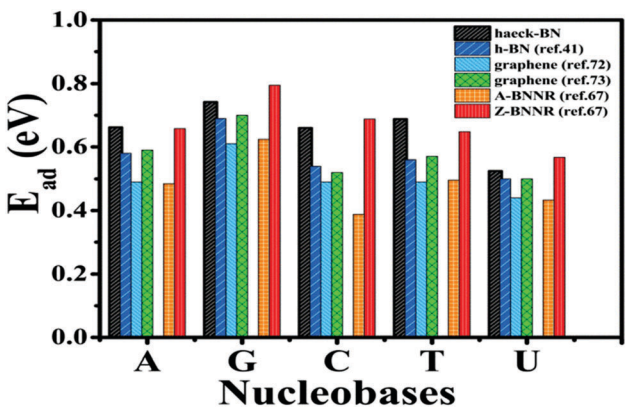

Fig. 7 Comparative adsorption energy plot of nucleobases with different nanostructures.

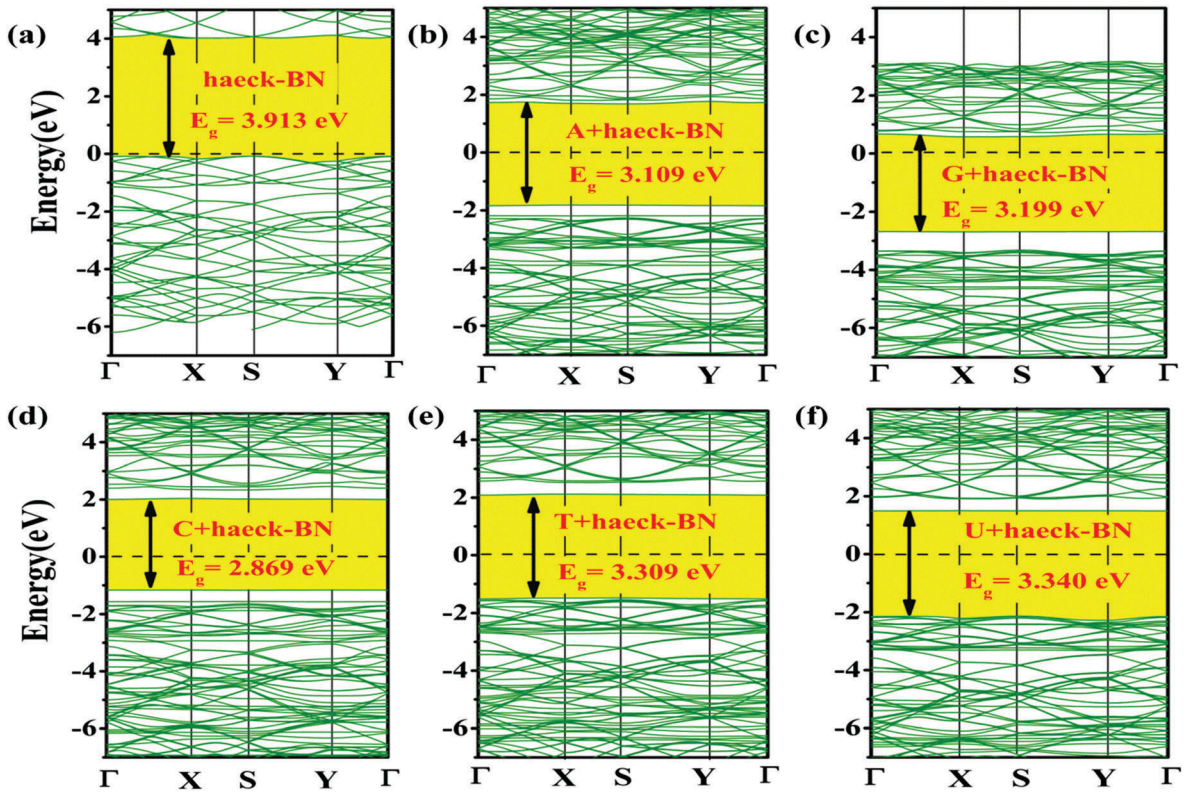

Fig. 8 Band structure plots of (a) pristine and nucleobase-adsorbed haeck-BN, (b) adenine (c) guanine (d) cytosine (e) thymine and (f) uracil.

representatives of any system's ability to donate or accept electron. In the collective form, they are known as frontier molecular orbitals. These orbitals are considered as the main orbitals involved in the chemical stability, and are situated on either side of the Fermi level, which also bring light to understanding the electronic state present near Fermi level and the transfer of electrons. The systematics of HOMO and LUMO orbitals for all considered systems are shown in Fig. S4 of the ESI.† From the figure, we can see that the electronic cloud in both orbitals of pristine haeck-BN is distributed over the entire structure. Electron cloud in HOMO is mainly due to the N atom, while that in LUMO is due to B atom throughout the structure. This indicates that the electron states near the Fermi level are due to p orbital of B and N atoms. These orbitals can capture or lose electrons. We see large differences in the HOMO and LUMO orbital electron clouds of pristine haeck-BN after the adsorption of nucleobases (Fig. S4, ESI†). In all nucleobase-adsorbed haeck-BN systems, the LUMOs are more localized on N and O atoms, which clearly indicates that the electron transfer mainly occurs between N and O atoms of the nucleobases and the HOMO orbitals of haeck-BN that are localized over B atoms.

To understand the molecular contribution in electronic properties, we calculated the density of states (DOS) and partial density of states (PDOS) of pristine and nucleobase-adsorbed haeck-BN, which are presented in Fig. 9 and Fig S1 (in the ESI†). The major advantage of DOS as well as PDOS calculation is that we can easily analyze the contribution of electronic states by the adsorbed molecule. Fig. 9 clearly shows that the valance band of pristine haeck-BN has the major contribution to the Fermi

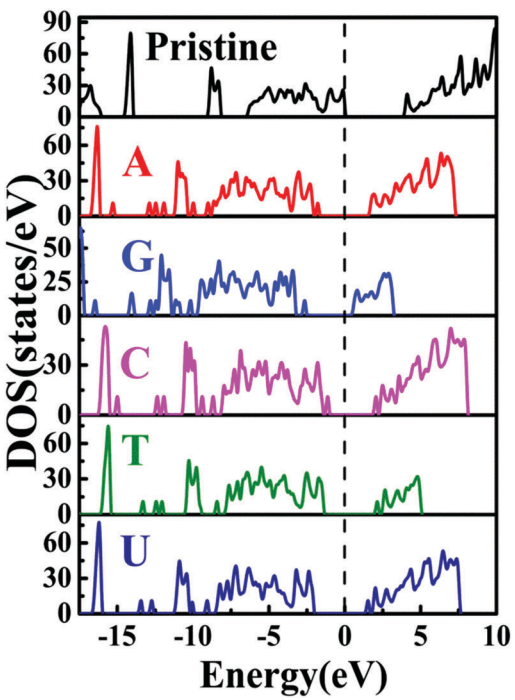

Fig. 9 Electronic density of states (DOS) plots of pristine haeck-BN along with nucleobase-adsorbed haeck-BN.

level. The interaction of haeck-BN with the nucleobases results in small peaks in the valence band region near Fermi level at −1.5 eV, −1.9 eV and −2.5 eV in case of C, A and G, respectively. However, among these three nucleobases, only C contributes to the conduction band. Some states are generated at 1.7 eV and 2 eV in the conduction band region in case of U and T, respectively. From the DOS data, it is clear that all the nucleobases alter the electronic properties of haeck-BN significantly with major contribution in the lower valence band region between −10 eV to −15 eV, where the impurity states have been generated from the interaction of molecules and haeck-BN. Major contribution arises from the p orbit electrons, which create the extra peak. Cytosine modulates the band gap of pristine haeck-BN by a large amount (1.04 eV) due to the appearance of some extra electronic states from the presence of NH_2 group in the molecule. Among all five nucleobases, guanine has the largest adsorption energy over haeck-BN due to its specific structural and electronic properties. The presence of oxygen atom in guanine, which is a strong electron donor, binds it strongly to the haeck-BN surface. The extra pentagon with C, N and O atoms induces the molecule to exhibit more polarization. The higher electronegativity of N and O atoms induces greater binding.[72,79]

The value of energy gap (E_g) is an important factor in ascertaining the electrical conductivity (σ) of materials because the energy required to remove an electron from the outer shell to become a free portable charge carrier is equivalent to the bandgap.

The classical relation between E_g and electrical conductivity of a material can be expressed by the following relation:[80]

$$\sigma \propto e^{\frac{-E_g}{2kT}} \quad (3)$$

where k and T are the Boltzmann's constant and the temperature respectively. According to eqn (3), conductivity is inversely proportional to the bandgap, indicating that smaller the value of bandgap E_g higher the electrical conductivity at a given temperature T. Thus, after the adsorption of nucleobases over the haeck-BN surface, a significant decrease in the band gap indicates an increase in σ of the haeck-BN sheet. σ increases in the order C → G → A → T → U-adsorbed haeck-BN. Therefore, after adsorption of nucleobases, the energy gap changes and becomes narrower. Consequently, conductivity of the nanosheet increases, confirming the strong interaction between the molecule and haeck-BN. The change in the Fermi level of haeck-BN due to the nucleobases causes an electrical signal, and therefore, it could be potentially used in biosensor applications.

In order to check the novelty of haeck-BN as a carrier of nucleobases and its reusability, we calculated the recovery time. The recovery time is a known parameter to decide the superiority of any sensor or detector or carrier with respect to other such devices. Generally, experimentalists find the recovery time by heating the substrate. However, the theoretical approach to estimate the recovery time is based on transition theory. The required equation can be expressed as[81]

$$\tau = \nu^{-1} e^{\frac{-E_{ads}}{kT}} \quad (4)$$

where ν is the attempt frequency, k is the Boltzmann constant ($\sim 8.318 \times 10^{-3}$ kJ mol^{-1} K^{-1}) and T is the temperature. We used the value of attempt frequency as 10^{12} s^{-1} [81–83] and temperature as 298 K, which has been employed to measure the recovery time for CNT from NO_2 molecule. Ultra-fast recovery time of 292 ms (millisecond), 130 ms, 120 ms, 160 ms and 0.6 ms was predicted for haeck-BN by using this attempt frequency for G, A, C, T and U, respectively.

We have also calculated the work function of pristine as well as nucleobase-adsorbed haeck-BN sheet to further check the sensing capability of nucleobases. The work function (ϕ (eV)) is the amount of energy required to remove an electron from the highest filled level in the Fermi distribution of any material to a point in a field-free zone just outside the solid at absolute zero temperature.[53]

$$\phi \text{ (eV)} = E_{vac} - E_F \quad (5)$$

where E_{vac} is the energy at vacuum level and E_F is Fermi level energy. By integrating the density of states from the lowest energy level to an energy level that gives the total number of electrons in a unit cell, we determined the Fermi energy level (E_F). E_{vac} was obtained by planar-average electrostatic potential energy along the z-direction, which is the direction of vacuum.[53] ϕ plots are shown in Fig. S2 of ESI.† There are two negative peaks on the curves of electrostatic potentials, and the strong and weak peaks correspond to the positions of haeck-BN nanosheet and the nucleobases, respectively. The difference in the electrostatic potentials between the Fermi and vacuum levels is the work function. ϕ for haeck-BN shows a significant decrease after the adsorption of nucleobases. ϕ of pristine haeck-BN was calculated as 5.972 eV, which was comparatively higher than that for other BN nanostructures.[68,84] A Large decrease in ϕ of haeck-BN was observed after the adsorption of nucleobase on its surface. The modulation of ϕ has the following trend: G (3.135 eV) > A (2.076 eV) ≈ U (2.058 eV) > C (1.517 eV) ≈ T (1.469 eV). The calculated work functions are shown in Table 2. The change in work function verifies that the physical adsorption of nucleobases on the surface of haeck-BN occurs due to strong nucleobase-haeck-BN interactions. The large decrease in the work function enhances photocatalysis since lower the work function leads to greater the catalytic activity. The modulation of electronic properties after adsorption of nucleobases on

Table 2 Adsorption energy E_{ad} (eV), vertical distance d (Å) of nucleobases from haeck-BN, bandgap E_g (eV) and Fermi energy E_F (eV)

System	haeck-BN	A	G	C	T	U
E_g (eV)	3.913	3.109	3.199	2.869	3.309	3.340
ΔE_g (eV)	—	0.714	0.914	1.044	0.604	0.573
E_{ad} (eV)	—	−0.662	−0.742	−0.660	−0.668	−0.525
d (Å)	—	2.945	2.745	2.775	2.725	2.953
E_F	−4.199	−1.617	−0.424	−2.322	−2.344	−1.798
Φ (eV)	5.972	3.896	2.837	4.455	4.503	3.914

haeck-BN is clearly evident in our results, which further suggest an easy detection of nucleobases by haeck-BN.

Finally, from the all abovementioned results, we can say that the nucleobase molecules get physically adsorbed on the haeck-BN surface. Thus, it is beneficial to utilize this new boron nitride cousin for targeted delivery of these biomolecule as reversibility is easy in case of physisorption than in chemisorption. Our results indicate that haeck-BN is a good candidate as a biomolecule carrier, and should be explored further for its biomedical and photocatalytic applications.

4. Conclusions

Using the state-of-the-art first principles calculations based on density functional theory, we investigated the electronic properties of the relatively newly proposed haeck-BN comprising square and octagonal rings. The kinetic stability of this haeckelite monolayer was confirmed by phonon dispersion curves and phonon density of states. There is not a single mode with imaginary frequency in the entire BZ. The calculated electronic properties of this new haeck-BN form illustrate its direct bang gap semiconducting behavior, which is the main advantage of any material utilized as a chemical as well as a biosensor. To understand the adsorption behavior of nucleobases on haeck-BN surface, we employed van der Waals corrections (DFT-D2) to the density functional theory. The comparative analysis of adsorption mechanism of nucleobases with those on graphene, BNNT and haeck-BN was discussed in detail, and haeck-BN was proven to show superior performance. Our results depict the physisorption of nucleobases on the surface of haeck-BN with the order G > T > A ≈ C > U. The change in work function after the adsorption of nucleobases was also calculated and changes were found in order G (3.135 eV) > A (2.076 eV) ≈ U (2.058 eV) > C (1.517 eV) ≈ T (1.469 eV), which is different from both graphene and BNNT. This further confirms the sensitivity of haeck-BN towards the nucleobases. For further confirmation of the novelty of the haeck-BN as a biosensor, we calculated the recovery time. Very low recovery times of 292 ms, 130 ms, 120 ms, 160 ms and 0.6 ms were predicted for G, A, C, T and U, respectively, which reinforced the possibility of haeck-BN as a reusable biosensor. The large change in the electronic properties confirms the interactions between haeck-BN and the nucleobases and hence, it is possible to use haeck-BN for the detection of these bio molecules. Thus, based on our results, we may conclude that haeck-BN may act as an alternative candidate to other h-BN and graphene systems for sensing application for nucleobases as well as DNA sequencing. We hope that our results will motivate more experimental and theoretical studies on new layered III–V semiconducting materials.

Conflicts of interest

There are no conflicts to declare.

Acknowledgements

The study was financially supported by a research project from Science and Engineering Research Board (SERB) (SR/S2/CMP-0005/2013), Govt. of India. The computations are carried out using high performance computer cluster provided under DST-FIST program.

Notes and references

1 W. Krätschmer, L. D. Lamb, K. Fostiropoulos and D. R. Huffman, Solid C60: a new form of carbon, *Nature*, 1990, **347**, 354–358.
2 D. S. Bethune, C. H. Kiang, M. S. de Vries, G. Gorman, R. Savoy, J. Vazquez and R. Beyers, Cobalt-catalysed growth of carbon nanotubes with single-atomic-layer walls, *Nature*, 1993, **363**, 605–607.
3 L. S. Ying, M. A. Bin Mohd Salleh, H. B. Mohamed Yusoff, S. B. Abdul Rashid and J. B. Abd Razak, Continuous production of carbon nanotubes - A review, *J. Ind. Eng. Chem.*, 2011, **17**, 367–376.
4 K. S. Novoselov, A. K. Geim, S. V. Morozov, D. Jiang, Y. Zhang, S. V. Dubonos, I. V. Grigorieva and A. A. Firsov, Electric Field Effect in Atomically Thin Carbon Films, *Science*, 2004, **306**, 666–669.
5 E. Pop, V. Varshney and A. K. Roy, Thermal properties of graphene: Fundamentals and applications, *MRS Bull.*, 2012, **37**, 1273–1281.
6 X. Wang, L. Zhi and K. Müllen, Transparent, conductive graphene electrodes for dye-sensitized solar cells, *Nano Lett.*, 2008, **8**, 323–327.
7 J. H. Chen, M. Ishigami, C. Jang, D. R. Hines, M. S. Fuhrer and E. D. Williams, Printed graphene circuits, *Adv. Mater.*, 2007, **19**, 3623–3627.
8 Y. Zhang, Y. W. Tan, H. L. Stormer and P. Kim, Experimental observation of the quantum Hall effect and Berry's phase in graphene, *Nature*, 2005, **438**, 201–204.
9 S. V. Morozov, K. S. Novoselov, M. I. Katsnelson, F. Schedin, D. C. Elias, J. A. Jaszczak and A. K. Geim, Giant intrinsic carrier mobilities in graphene and its bilayer, *Phys. Rev. Lett.*, 2008, **100**, 016602.
10 J. H. Chen, C. Jang, S. Adam, M. S. Fuhrer, E. D. Williams and M. Ishigami, Charged-impurity scattering in graphene, *Nat. Phys.*, 2008, **4**, 377–381.
11 S. S. Gregersen, S. R. Power and A. P. Jauho, Nanostructured graphene for spintronics, *Phys. Rev. B: Condens. Matter Mater. Phys.*, 2017, **95**, 121406.
12 F. Molitor, J. Güttinger, C. Stampfer, S. Dröscher, A. Jacobsen, T. Ihn and K. Ensslin, Electronic properties of graphene nanostructures, *J. Phys.: Condens. Matter*, 2011, **23**, 243201.
13 J. Klinovaja and D. Loss, Spintronics in MoS_2 monolayer quantum wires, *Phys. Rev. B: Condens. Matter Mater. Phys.*, 2013, **88**, 075404.
14 Y. Xu, Z. Gan and S. C. Zhang, Enhanced thermoelectric performance and anomalous seebeck effects in topological insulators, *Phys. Rev. Lett.*, 2014, **112**, 226801.

15 Y. N. Xu and W. Y. Ching, Calculation of ground-state and optical properties of boron nitrides in the hexagonal, cubic, and wurtzite structures, *Phys. Rev. B: Condens. Matter Mater. Phys.*, 1991, **44**, 7787–7798.

16 W. Choi, N. Choudhary, G. H. Han, J. Park, D. Akinwande and Y. H. Lee, Recent development of two-dimensional transition metal dichalcogenides and their applications, *Mater. Today*, 2017, **20**, 116–130.

17 K. Takeda and K. Shiraishi, Theoretical possibility of stage corrugation in Si and Ge analogs of graphite, *Phys. Rev. B: Condens. Matter Mater. Phys.*, 1994, **50**, 14916–14925.

18 S. Cahangirov, M. Topsakal, E. Aktürk, H. Šahin and S. Ciraci, Two- and one-dimensional honeycomb structures of silicon and germanium, *Phys. Rev. Lett.*, 2009, **102**, 236804.

19 H. Liu, A. T. Neal, Z. Zhu, Z. Luo, X. Xu, D. Tománek and P. D. Ye, Phosphorene: An unexplored 2D semiconductor with a high hole mobility, *ACS Nano*, 2014, **8**, 4033–4041.

20 S. B. Pillai, S. Narayan, S. D. Dabhi and P. K. Jha, First principles calculation of two dimensional antimony and antimony arsenide, *AIP Conf. Proc.*, 2016, **1731**, 090024.

21 S. B. Pillai, S. D. Dabhi, S. Narayan and P. K. Jha, Strain Effect on Electronic and Lattice Dynamical Behaviour of Two Dimensional Bi, BiAs and BiSb, *AIP Conf. Proc.*, 2018, **1942**, 090022.

22 B. Feng, J. Zhang, Q. Zhong, W. Li, S. Li, H. Li, P. Cheng, S. Meng, L. Chen and K. Wu, Experimental realization of two-dimensional boron sheets, *Nat. Chem.*, 2016, **8**, 563–568.

23 A. Pakdel, C. Zhi, Y. Bando and D. Golberg, Low-dimensional boron nitride nanomaterials, *Mater. Today*, 2012, **15**, 256–265.

24 J. Yin, L. Jidong, Y. Hang, Y. Jin, G. Tai, L. Xuemei, Z. Zhang and W. Guo, Boron Nitride Nanostructures: Fabrication, Functionalization and Applications, *Small*, 2016, **12**, 2942–2968.

25 A. Pakdel, Y. Bando and D. Golberg, Nano boron nitride flatland, *Chem. Soc. Rev.*, 2014, **43**, 934–959.

26 C. R. Dean, A. F. Young, I. Meric, C. Lee, L. Wang, S. Sorgenfrei, K. Watanabe, T. Taniguchi, P. Kim, K. L. Shepard and J. Hone, Boron nitride substrates for high-quality graphene electronics, *Nat. Nanotechnol.*, 2010, **5**, 722–726.

27 P. Sutter, J. Lahiri, P. Zahl, B. Wang and E. Sutter, Scalable synthesis of uniform few-layer hexagonal boron nitride dielectric films, *Nano Lett.*, 2013, **13**, 276–281.

28 X. Li, J. Yin, J. Zhou and W. Guo, Large area hexagonal boron nitride monolayer as efficient atomically thick insulating coating against friction and oxidation, *Nanotechnology*, 2014, **25**, 105701.

29 G. H. Lee, Y. J. Yu, C. Lee, C. Dean, K. L. Shepard, P. Kim and J. Hone, Electron tunneling through atomically flat and ultrathin hexagonal boron nitride, *Appl. Phys. Lett.*, 2011, **99**, 243114.

30 Q. Li, X. Zou, M. Liu, J. Sun, Y. Gao, Y. Qi, X. Zhou, B. I. Yakobson, Y. Zhang and Z. Liu, Grain Boundary Structures and Electronic Properties of Hexagonal Boron Nitride on Cu(111), *Nano Lett.*, 2015, **15**, 5804–5810.

31 Y. Liu, X. Zou and B. I. Yakobson, Dislocations and Grain Boundaries in Two-Dimensional Boron Nitride, *ACS Nano*, 2012, **6**, 7053–7058.

32 D. C. Camacho-Mojica and F. López-Urías, GaN Haeckelite Single-Layered Nanostructures: Monolayer and Nanotubes, *Sci. Rep.*, 2015, **5**, 1–11.

33 P. V. Gaikwad, P. K. Pujari, S. Chakroborty and A. Kshirsagar, Cluster assembly route to a novel octagonal two-dimensional ZnO monolayer, *J. Phys.: Condens. Matter*, 2017, **29**, 335501.

34 X. Tu, S. Manohar, A. Jagota and M. Zheng, DNA sequence motifs for structure-specific recognition and separation of carbon nanotubes, *Nature*, 2009, **460**, 250–253.

35 D. Umadevi and G. N. Sastry, Quantum mechanical study of physisorption of nucleobases on carbon materials: Graphene versus carbon nanotubes, *J. Phys. Chem. Lett.*, 2011, **2**, 1572–1576.

36 C. Zhi, Y. Bando, W. Wang, C. Tang, H. Kuwahara and D. Golberg, DNA-mediated assembly of boron nitride nanotubes, *Chem. – Asian J.*, 2007, **2**, 1581–1585.

37 G. Ciofani, V. Raffa, A. Menciassi and A. Cuschieri, Cytocompatibility, interactions, and uptake of polyethyleneimine-coated boron nitride nanotubes by living cells: Confirmation of their potential for biomedical applications, *Biotechnol. Bioeng.*, 2008, **101**, 850–858.

38 X. Chen, P. Wu, M. Rousseas, D. Okawa, Z. Gartner, A. Zettl and C. R. Bertozzi, Boron Nitride Nanotubes Are Noncytotoxic and Can Be Functionalized for Interaction with Proteins and Cells, *J. Am. Chem. Soc.*, 2009, **131**, 890–891.

39 S. Liu, B. Lu, Q. Zhao, J. Li, T. Gao, Y. Chen, Y. Zhang, Z. Liu, Z. Fan, F. Yang, L. You and D. Yu, Boron nitride nanopores: Highly sensitive DNA single-molecule detectors, *Adv. Mater.*, 2013, **25**, 4549–4554.

40 L. Zhang and X. Wang, DNA Sequencing by Hexagonal Boron Nitride Nanopore: A Computational Study, *Nanomaterials*, 2016, **6**, 111–121.

41 Y. Zhao, Y. Xie, Z. Liu, X. Wang, Y. Chai and F. Yan, Two-dimensional material membranes: An emerging platform for controllable mass transport applications, *Small*, 2014, **10**, 4521–4542.

42 Q. Lin, X. Zou, G. Zhou, R. Liu, J. Wu, J. Li and W. Duan, Adsorption of DNA/RNA nucleobases on hexagonal boron nitride sheet: an ab initio study, *Phys. Chem. Chem. Phys.*, 2011, **13**, 12225–12230.

43 K. Jin, L. Xie, Y. Tian and D. Liu, Au-Modified Monolayer MoS_2 Sensor for DNA Detection, *J. Phys. Chem. C*, 2016, **120**, 11204–11209.

44 G. Ciofani, V. Raffa, J. Yu, Y. Chen, Y. Obata, S. Takeoka, A. Menciassi and A. Cuschieri, Boron Nitride Nanotubes: A Novel Vector for Targeted Magnetic Drug Delivery, *Curr. Nanosci.*, 2009, **5**, 33–38.

45 G. G. Genchi and G. Ciofani, Bioapplications of boron nitride nanotubes, *Nanomedicine*, 2015, **10**, 3315–3319.

46 Z. Zhang, H. Huang, X. Yang and L. Zang, Tailoring electronic properties of graphene by π–π Stacking with aromatic molecules, *J. Phys. Chem. Lett.*, 2011, **2**, 2897–2905.

47 T. Kar, H. F. Bettinger, S. Scheiner and A. K. Roy, Noncovalent π-π Stacking and CH$\cdots\pi$ Interactions of Aromatics on the Surface of Single-Wall Carbon Nanotubes: An MP2 Study, *J. Phys. Chem. C*, 2008, **112**, 20070–20075.

48 P. Giannozzi, S. Baroni, N. Bonini, M. Calandra, R. Car, C. Cavazzoni, D. Ceresoli, G. L. Chiarotti, M. Cococcioni, I. Dabo, A. Dal Corso, S. De Gironcoli, S. Fabris, G. Fratesi, R. Gebauer, U. Gerstmann, C. Gougoussis, A. Kokalj, M. Lazzeri, L. Martin-Samos, N. Marzari, F. Mauri, R. Mazzarello, S. Paolini, A. Pasquarello, L. Paulatto, C. Sbraccia, S. Scandolo, G. Sclauzero, A. P. Seitsonen, A. Smogunov, P. Umari and R. M. Wentzcovitch, QUANTUM ESPRESSO: A modular and open-source software project for quantum simulations of materials, *J. Phys.: Condens. Matter*, 2009, **21**, 395502.

49 J. D. Head and M. C. Zerner, A Broyden-Fletcher-Goldfarb-Shanno optimization procedure for molecular geometries, *Chem. Phys. Lett.*, 1985, **122**, 264–270.

50 J. P. Perdew, K. Burke and M. Ernzerhof, Generalized Gradient Approximation Made Simple, *Phys. Rev. Lett.*, 1996, **77**, 3865–3868.

51 H. J. Monkhorst and J. D. Pack, Special points for Brillouin-zone integrations, *Phys. Rev. B: Solid State*, 1976, **13**, 5188–5192.

52 S. Baroni, S. De Gironcoli, A. Dal Corso and P. Giannozzi, Phonons and related crystal properties from density-functional perturbation theory, *Rev. Mod. Phys.*, 2001, **73**, 515–562.

53 C. Kittel, *Introduction to Solid State Physics*, John Wiley & Sons, Inc, United States, 2010.

54 S. Grimme, Semiempirical GGA-Type Density Functional Constructed with a Long-Range Dispersion Correction, *J. Comput. Chem.*, 2006, **27**, 1787–1799.

55 M. Topsakal, E. Aktürk and S. Ciraci, First-principles study of two- and one-dimensional honeycomb structures of boron nitride, *Phys. Rev. B: Condens. Matter Mater. Phys.*, 2009, **79**, 115442.

56 E. Kroumova, M. L. Aroyo, J. M. Perez-Mato, A. Kirov, C. Capillas, S. Ivantchev and H. Wondratschek, Bilbao Crystallographic Server: Useful databases and tools for phase-transition studies, *Phase Transitions*, 2003, **76**, 155–170.

57 S. Barua, H. S. Dutta, S. Gogoi, R. Devi and R. Khan, Nanostructured MoS_2 Based Advanced Biosensors: A Review, *ACS Appl. Nano Mater.*, 2018, **1**, 2–25.

58 P. Anees, M. C. Valsakumar and B. K. Panigrahi, Effect of strong phonon–phonon coupling on the temperature dependent structural stability and frequency shift of 2D hexagonal boron nitride, *Phys. Chem. Chem. Phys.*, 2016, **18**, 2672–2681.

59 P. K. Jha and H. R. Soni, Strain induced modification in phonon dispersion curves of monolayer boron pnictides, *J. Appl. Phys.*, 2014, **115**, 023509.

60 I. Lifshitz, Thermal properties of chain and layered structures at low temperatures, *Zh. Eksp. Teor. Fiz.*, 1952, **22**, 475–486.

61 M. S. Dresselhaus, *Physical Properties of Carbon Nanotubes*, Imperial College Press, London, 2005.

62 C. Marchbanks and Z. Wu, Reduction of heat capacity and phonon group velocity in silicon nanowires, *J. Appl. Phys.*, 2015, **117**, 084305.

63 J.-Y. Lin, P. L. Ho, H. L. Huang, P. H. Lin, Y.-L. Zhang, R.-C. Yu, C.-Q. Jin and H. D. Yang, BCS-like superconductivity in $MgCNi_3$, *Phys. Rev. B: Condens. Matter Mater. Phys.*, 2003, **67**, 052501.

64 P. K. Jha and S. P. Sanyal, A lattice dynamical study of the role of pressure on Raman modes in high-T_c $HgBa_2CuO_4$, *Phys. C*, 1996, **261**, 259–262.

65 P. K. Jha, Phonon spectra and vibrational mode instability of $MgCNi_3$, *Phys. Rev. B: Condens. Matter Mater. Phys.*, 2005, **72**, 214502.

66 W. Lu, X. Liu, S. Liu, W. Cao, Y. Zhang and P. Yang, Locus-specific Retention Predictor (LsRP): A Peptide Retention Time Predictor Developed for Precision Proteomics, *Sci. Rep.*, 2017, **7**, 1–9.

67 E. C. Anota, Y. Tlapale, M. S. Villanueva and J. A. R. Márquez, Non-covalent functionalization of hexagonal boron nitride nanosheets with guanine, *J. Mol. Model.*, 2015, **21**, 215–221.

68 S. D. Dabhi, B. Roondhe and P. K. Jha, Nucleobases-decorated boron nitride nanoribbons for electrochemical biosensing: A dispersion-corrected DFT study, *Phys. Chem. Chem. Phys.*, 2018, **20**, 8943–8950.

69 B. Roondhe, S. D. Dabhi and P. K. Jha, Sensing properties of pristine boron nitride nanostructures towards alkaloids: A first principles dispersion corrected study, *Appl. Surf. Sci.*, 2018, **441**, 588–598.

70 S. Grimme, J. Antony, S. Ehrlich and H. Krieg, A consistent and accurate ab initio parametrization of density functional dispersion correction (DFT-D) for the 94 elements H-Pu, *J. Chem. Phys.*, 2010, **132**, 154104.

71 J. B. A. Davis, F. Baletto and R. L. Johnston, The Effect of Dispersion Correction on the Adsorption of CO on Metallic Nanoparticles, *J. Phys. Chem. A*, 2015, **119**, 9703–9709.

72 N. Ding, X. Chen, C.-M. L. Wu and H. Li, Adsorption of nucleobase pairs on hexagonal boron nitride sheet: hydrogen bonding versus stacking, *Phys. Chem. Chem. Phys.*, 2013, **15**, 10767–10776.

73 S. Gowtham, R. H. Scheicher, R. Ahuja, R. Pandey and S. P. Karna, Physisorption of nucleobases on graphene: Density-functional calculations, *Phys. Rev. B: Condens. Matter Mater. Phys.*, 2007, **76**, 033401.

74 H. H. Gürel and B. Salmankurt, Binding mechanisms of DNA/RNA nucleobases adsorbed on graphene under charging: First-principles van der Waals study, *Mater. Res. Express*, 2017, **4**, 065401.

75 P. Han, K. Akagi, F. Federici Canova, H. Mutoh, S. Shiraki, K. Iwaya, P. S. Weiss, N. Asao and T. Hitosugi, Bottom-up graphene-nanoribbon fabrication reveals chiral edges and enantioselectivity, *ACS Nano*, 2014, **8**, 9181–9187.

76 K. Müller-Dethlefs and P. Hobza, Noncovalent Interactions: A Challenge for Experiment and Theory, *Chem. Rev.*, 2000, **100**, 143–168.

77 S. Mukhopadhyay, S. Gowtham and R. H. Scheicher, Theoretical study of physisorption of nucleobases on boron nitride nanotubes: a new class of hybrid nano-biomaterials, *Nanotechnology*, 2010, **21**, 165703.

78 Z. Gulácsi, Interaction-created effective flat bands in conducting polymers, *Eur. Phys. J. B*, 2014, **87**, 143–153.

79 F. Erkoç and Sakir Erkoç, Structural and electronic properties of guanine and guanosine, *THEOCHEM*, 2002, **589**, 405–411.
80 S. S. Li, *Semiconductor Physical Electronics*, Springer Science, United States, 1997.
81 Z. Rostami, M. Pashangpour and R. Moradi, DFT study on the chemical sensing properties of $B_{24}N_{24}$ nanocage toward formaldehyde, *J. Mol. Graphics Modell.*, 2017, **72**, 129–135.
82 S. Peng, K. Cho, P. Qi and H. Dai, Ab initio study of CNT NO_2 gas sensor, *Chem. Phys. Lett.*, 2004, **387**, 271–276.
83 K. Patel, B. Roondhe, S. D. Dabhi and P. K. Jha, A new flatland buddy as toxic gas scavenger: A first principles study, *J. Hazard. Mater.*, 2018, **351**, 337–345.
84 F. Schulz, R. Drost, S. K. Hämäläinen, T. Demonchaux, A. P. Seitsonen and P. Liljeroth, Epitaxial hexagonal boron nitride on Ir(111): A work function template, *Phys. Rev. B: Condens. Matter Mater. Phys.*, 2014, **89**, 235429.

ACS APPLIED NANO MATERIALS
Cite This: ACS Appl. Nano Mater. 2019, 2, 1552−1561
Article
www.acsanm.org

Neurotransmitter-Functionalized Boron Nitride Nanoribbons as Biological Cargo Carriers: Analysis by Density Functional Theory

Basant Roondhe[†] and Prafulla K Jha*[,†]

[†]Department of Physics, Faculty of Science, The Maharaja Sayajirao University of Baroda, Vadodara 390002, India

Supporting Information

ABSTRACT: The structural and electronic properties of boron nitride nanoribbons (BNNRs) adsorbed with two neurotransmitters, dopamine (DA) and adrenaline (AD), have been systematically investigated using electronic structure calculations based on density functional theory to test the feasibility of using BNNRs as a carrier for neurotransmitter (NRT). In order to check the adsorption mechanism of AD and DA on BNNRs, a comparative study onto armchair BNNR (ABNNR) and zigzag BNNR (ZBNNR) was assessed using dispersion corrected density functional theory. Our study reveals that the adsorption of both NRTs effectively modulates the electronic structure of ABNNR and ZBNNR. There is a strong interaction of DA and AD with both BNNRs. However, the AD and DA binds more strongly to ABNNR with the values of −1.013 and −1.144 eV, respectively. DA and AD adsorption on BNNRs significantly modulates the work function of pristine BNNRs. The results of our systematic study aims to understand the impact of BNNRs on NRTs in bio-nano interface and can be used as carrier for neurological medicines, which will further open new perspectives to design new sequencing by undertaking human health as well as live cells.

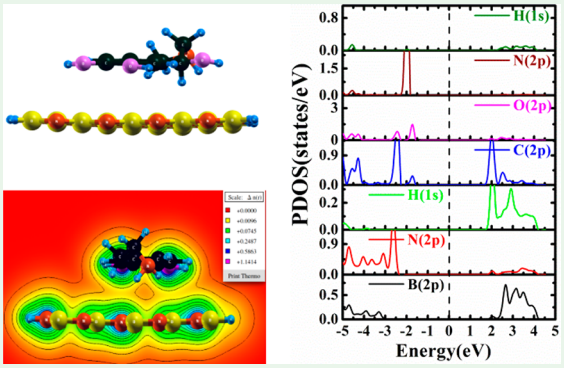

KEYWORDS: *neurotransmitters, BNNRs, adsorption mechanism, work function, density functional theory*

INTRODUCTION

An objective of nanotechnology is to gather information on materials at the molecular level using nanoscopic sized electronic devices. Researchers from all over the world are fabricating devices to detect molecules at ultralow concentration. A major breakthrough in the development of nanodetectors was realized with the discovery of the two-dimensional material graphene.[1−3] With its sp^2 C−C bonding,[4] it consists of extraordinary electronic and transport properties, an extremely high surface-to-volume ratio which inspires researchers to consider other two-dimensional materials with the same hybridization as graphene. Till now, monolayers of hexagonal boron nitride (h-BN), transition metal sulfides, phosphorus, silicon, and many other materials have been synthesized or predicted.[5−9] The closest structural analogue to carbon allotrope is boron nitride (BN).[5] Boron (group III) and nitrogen (group V) contribute equally in boron nitride structures. The three different isomers of BN similar to carbon are 3D cubic boron nitride (c-BN), 2D hexagonal boron nitride sheet (h-BN), 1D boron nitride nanotube (BNNT), and boron nitride nanoribbon (BNNR).[10] The major advantage of BN nanostructures (BNNs) over graphene is their wide band gap semiconducting nature which is absent in graphene and makes BNNs more suitable for sensors and nanoelectronics.[11,12]

Among all BNNs, boron nitride nanoribbon has gathered much attention due to its exceptional magnetic, electronic and optical properties along with good thermal stability gifted by its edge structure and is better than its carbon counterpart graphene nanoribbon GNR.[13] Although the structure is similar, the properties of BNNR are tremendously different from GNR due to B−N bonding nature. BNNR comprises hexagonal rings having every N atom bonded to three B atoms and vice versa in the planar form with strong directional bonding. The electron density in the π-orbital is localized closer to N atom than B atom, as each B atom has one to two electrons which is further shared with its three neighboring N atoms.[14] The hurdle in the path of its fabrication was succeeded by Zeng and co-workers through the well-established arc plasma etching method previously used to make GNR from CNT.[15] The lack of high aspect ratio ribbons, a major drawback of above method, was overcome by Erickson et al.[16] who developed an efficient process to fabricate BNNRs from BNNT. The structure of BNNR has different armchair (A), zigzag (Z), and chiral (C) edges like morphology which are similar to GNR but with remarkable electronic and magnetic properties, depending on edge atom and hydrogen passivation in BNNR.[17,18] Several reports suggest tuning of electronic properties of BNNRs for their potential applications in electronic, piezoelectric, photovoltaic, and optoelectronic

Received: January 6, 2019
Accepted: February 12, 2019
Published: February 12, 2019

DOI: 10.1021/acsanm.9b00028
ACS Appl. Nano Mater. 2019, 2, 1552−1561

devices and their different behavior compared to GNRs.[19−25] Additionally, the effect of strain on electronic properties of BNNRs was studied widely.[19,20,26,27] The dominance of BNNRs over GNRs arising from their capability to tune the properties makes them yearn for nanomaterial in biosensing applications. There are various reports on noncytotoxicity of BNNs.[28−31] The use of several coatings and surface treatments makes it difficult to compare the studies and identify equivocal threshold for time of exposure and maximum doses. Most recently, a study by Mateti et al.[32] shows contradictory results which can be attributed to the fact that the coatings/surfactants that are used together with BN cannot be expected to deliver the same results on all cell lines. The pristine forms of BN without coatings or surfactants are biocompatible in vitro and in vivo thereby representing BN as a base 2D material for bioapplications.[28,29] Once the clinical guidelines get defined for the most relevant biocompatibility parameters, different strategies can be adopted to engineer the BN nanostructures for specific applications like imaging, drug delivery, and stimulation.[30,31]

In recent times many health issues have arisen due to the neurological imbalance of NRTs. NRTs are the main chemicals responsible for the transmittance of signals between neuron cells.[33] It acts as a chemical messenger in our nervous system which passes the information by relaying it across synapses by mean of excitation of near neuron or the targeted tissue.[34] One type is monoamines, which consist of AD, DA, histamine, melatonin, noradrenaline, and serotonin.[35] It contains one amino group of aromatic ring connected with two carbon chain ($-CH_2-CH_2-$) and has the ability of NRT as well as neuromodulators. The main component in all monoamine based NRTs is its aromatic amino acids. Among all NRTs dopamine (DA) and adrenalin (AD) have a significant importance.

DA belongs to the families of phenethylamine and catecholamine which plays a significant role in several brain and body functions. L-DOPA is a chemical precursor from which, by removing a carboxyl group, DA is synthesized in the kidneys and brain. The DA is released in the brain and highly linked with reward mechanism which helps to motivated behavior. There are many ways to increase the formation of DA in brain, but the worst comes with the addiction of drugs. The abnormality in the amount of DA production causes much serious neurological disorder. Lack of DA production in brain can cause illness like Parkinson's disease, attention deficit hyperactive disorder, HIV infections, restless leg syndrome, and schizophrenia.[36−39] Another important NRT is AD or epinephrine which belongs to the catecholamine family and plays an important role in the nervous system of all mammals. Its major role is to control a wide variety of behavior as well as physiological process with the help of different receptors. Both NRTs are essential, and their imbalance level in the body embraces many diseases. During the past decade numerous researchers have attempted to make an improved and efficient sensor to monitor and measure these molecules.[12,40−49]

The determination or detection of NRTs is done by very expensive methods and in a controlled environment.[50−54] This makes it difficult to detect and to monitor; for this reason a simple and highly sensitive method is needed which can be achieved by electrochemical sensor.[50] There are many experimental as well as theoretical studies performed for the development of electrochemical sensor based on nanomaterial for NRTs.[55−58] The information on molecular level is the main aim to utilize the nanotechnology in the development of nanoscopic electronic devices. A recent study by Ortiz-Medina et al.[55] reported on a low dimensional DA sensor based on graphene (doped and defected) and analyzed the effects of electric field on the sensing of DA over graphene. Feng et al.[56] constructed a DA biosensor based on 3D N-doped graphene porous foam while Rossi Fernández et al.[57] described the noncovalent interaction of DA with pristine and defected graphene. The sensing ability of 2D h-BN toward DA with different surfactant to improve the sensing mechanism was systematically studied by Khan.[58] There are several studies focusing on DA detection, but to the best of our knowledge there does not exist any report on AD sensor. There has not been a focused study on the utilization of boron nitride nanostructures especially BNNR for electrochemical sensor for NRTs (DA and AD). The lack of molecular level understanding involved in the interaction on DA as well as AD sensors motivates us to explore BNNRs as a NRT sensor. The main aim of the present work is to investigate the sensing ability of BNNR toward DA and AD by adsorption energy calculation and also to understand the effect of the geometry of BNNR (ABNNR and ZBNNR) on the adsorption.

COMPUTATIONAL METHODOLOGY

The present study is done under the framework of first-principle calculations based on density functional theory (DFT). DFT solves the Schrödinger's equation for any particular system like molecules, nanostructures, solids, surfaces, and interfaces to determine the energy functional and its associated potential, which involves a greater effort than a direct solution for the energy. Excellent approximations are required to determine exact properties of the universal functionals for using it in unbiased and thus predictive studies, properties associated with an ab initio theory which further do not include fitting the model to experimental data. The ground state optimization is done using Quantum Espresso (QE) simulation package.[59] The Broyden−Fletcher−Goldfarb−Shanno (BFGS)[60] method is used with ultrasoft (US) Rappe−Rabe−Kaxiras−Joannopoulos (RRKJ) pseudopotential combined with suitable generalized gradient approximation (GGA) as exchange−correlation functional.[61] The interactions of molecule over the surface of BNNRs are studied by calculating the adsorption energy. The GGA functional predicts more accurately the interaction (adsorption) energy than LDA functional.[62,63] Since GGA depends on the local density as well as on the spatial variation of the density, it has been widely used for binding energy calculations. Hence, we have used GGA in our binding energy calculations, being the sensitive part of our study. The plane wave basis set with kinetic energy and charge density cutoffs of 60 and 600 Ry, respectively, are used for single particle functions, sufficient to obtain a good convergence. Uniform Monkhorst and Pack[64] k-point grids of size $1 \times 1 \times 16$ are taken in Brillouin zone (BZ) for the better evaluation of adsorption and electronic properties. The violation of charge neutrality less than $0.009e$ for the adequate convergence of the calculations is guaranteed by this k-point mesh. The ground state configuration of pristine BNNR has 1.45 Å average bond lengths between boron and nitrogen. A comparative analysis of the interactions of both NRTs (AD and DA) with BNNR having zigzag and armchair chirality is carried out first by full structural optimization, electronic band structure and adsorption energy calculations, density of states (DOS) plots along with partial

DOI: 10.1021/acsanm.9b00028
ACS Appl. Nano Mater. 2019, 2, 1552−1561

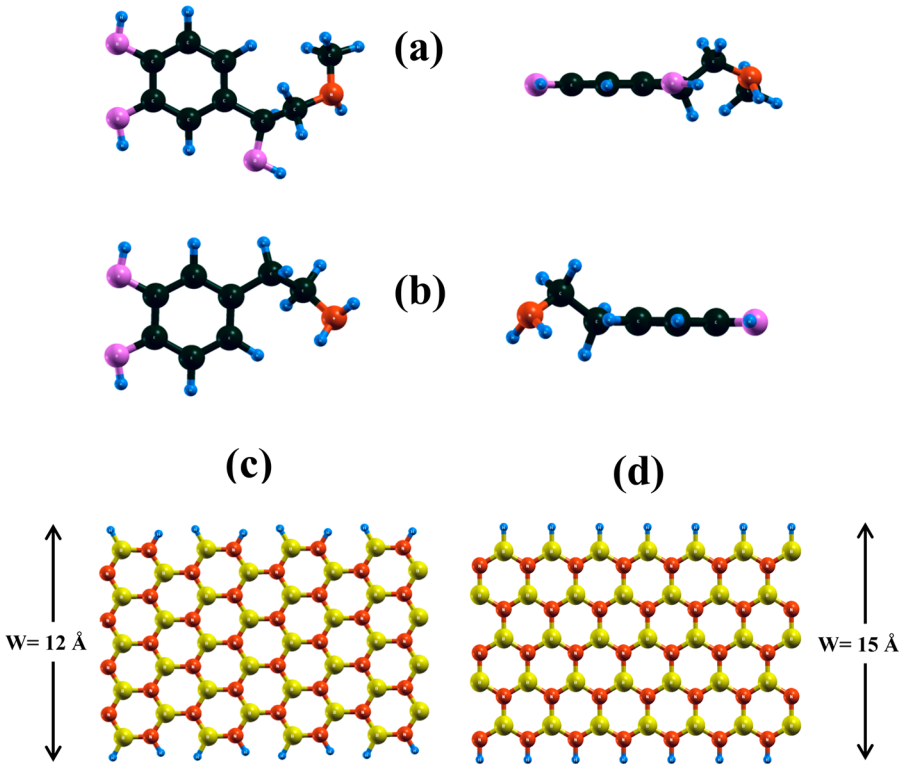

Figure 1. Optimized structure of (a) adrenaline, (b) dopamine, (c) ABNNR, and (d) ZBNNR. Oxygen, carbon, hydrogen, boron, and nitrogen are represented as pink, black, blue, yellow, and orange balls, respectively. *W* is the width of both nanoribbons.

density of states (PDOS), and work function calculations. Previous works on the adsorption of molecules on the nanosurface proved that accounting for the dispersion forces is necessary.[65−67] For this reason we have chosen a computational method which considers the correct description of long-range electron correlation. In the present study, we have employed Grimme's dispersion correction (DFT-D2)[68] which simply adds pairwise term of long-range behavior C_{6ij}/R_{ij}^6 in DFT energy, where C_{6ij} is the dispersion coefficient and the term R_{ij}^6 is the distance between the atoms. DFT-D2 can explain the noncovalent, long distance van der Waals interaction (i.e., ∼2.7 Å) between the adsorbent and the adsorbate. We have not adopted DFT-D3 in our calculation, as results obtained by DFT-D3 for noncovalent interaction between the adsorbent and the adsorbate are comparable with results obtained from DFT-D2.[69] The adsorption energy E_{ad} for NRTs over BNNRs has been calculated according to the following equation:

$$E_{ad} = E_{(BNNRs+NRT)} - \{E_{(BNNRs)} + E_{(NRT)}\} \quad (1)$$

where $E_{(BNNRs+NRT)}$ is the total energy of BNNRs adsorbed by NRT (AD and DA), $E_{(BNNRs)}$ is the total energy of the adsorbent nanoribbon, $E_{(NRT)}$ is the total energy of NRT (AD and DA) obtained from their full optimized geometries. Adsorption is defined as exergonic if $E_{ad} < 0$. We performed two independent calculations corresponding to periodic system and for molecules. The calculation of periodic system has been done using plane wave basis set with inclusion of DFT-D2, and the HOMO−LUMO energies of molecules are calculated using all-electron basis set with HSE06 functional making correct combination of a modeled system and functional used. The molecule adsorbed on supercell of BNNR brings the overall system in the domain of periodic systems; hence for accurate results calculations of molecules adsorbed over BNNR are performed using plane wave basis. However, for calculations involving only molecules we have used all-electron basis set for calculations as no periodic systems are involved. Hence the results obtained for periodic systems and individual molecules are reliable owing to the usage of appropriate functionals. Further, in order to examine the highest occupied molecular orbitals (HOMO) and lowest unoccupied molecular orbitals (LUMO), DA and AD are fully optimized at the HSE06 level using 6-31+G(D) basis set in Gaussian 09 suite of package.[70,71] For the accuracy of HOMO and LUMO levels single point calculations are also performed at the same level of theory. Optimized geometries for both molecules are confirmed to be in true minima by no imaginary frequencies.

RESULTS AND DISCUSSION

To understand the interaction between NRT and boron nitride nanoribbons (ABNNR and ZBNNR), we first performed full structural optimization of DA, AD, ABNNR, and ZBNNR individually and presented them in Figure 1. In our previous work, we have checked the dynamical stability of both types of BNNRs[66] and found no imaginary vibrational mode in the entire Brillouin zone, and hence the systems are in local minima. The phonon calculations for the whole boron nitride nanoribbon systems and neurotransmitter molecule are computationally quite costly as well as time consuming. Hence, not having phonon calculations for entire system is not a serious drawback as the main concern of this study is to have a system with local minima over which adsorption is to be done. Both BNNRs are multiplied in *z*-direction as it is periodic in *z*-axis; we have considered 1 × 1 × 4 supercell of ABNNR with 88 atoms and 1 × 1 × 7 supercell for ZBNNR

DOI: 10.1021/acsanm.9b00028
ACS Appl. Nano Mater. 2019, 2, 1552−1561

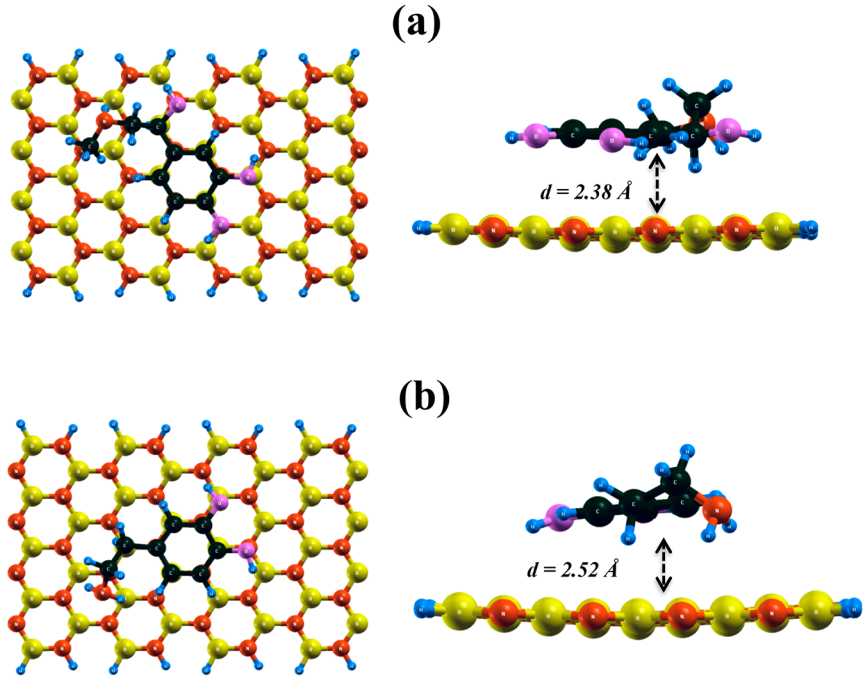

Figure 2. Optimized structure of ABNNR adsorbed with (a) adrenaline and (b) dopamine. The distance between the molecules and BNNRs is represented by *d*.

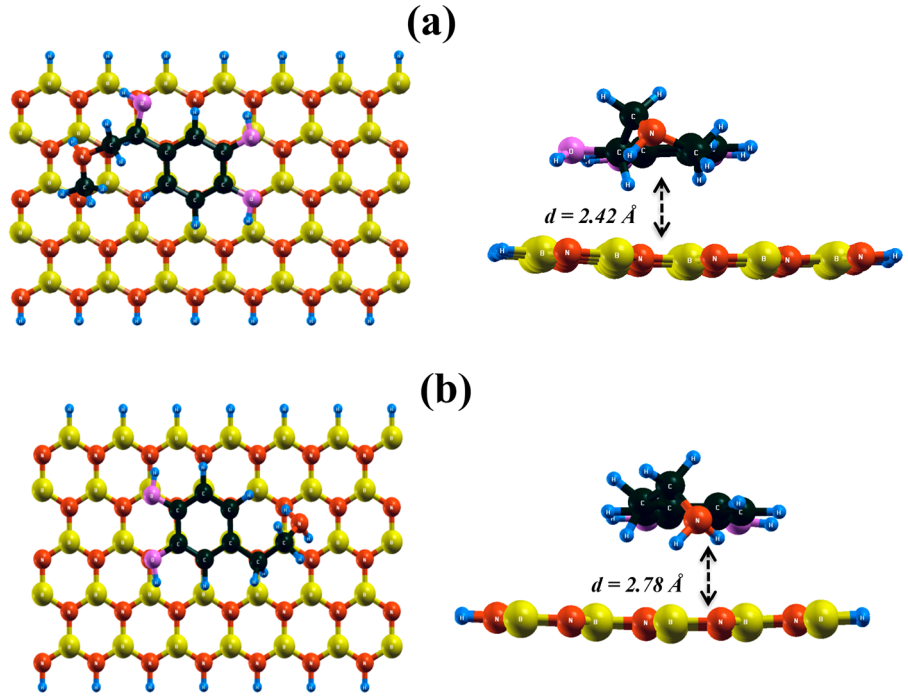

Figure 3. Optimized structure of ZBNNR adsorbed with (a) adrenaline and (b) dopamine. The distance between the molecules and BNNRs is represented by *d*.

with 84 atoms for providing large surface to interact with molecules.

After optimization, the width of ABNNR and ZBNNR is 12 and 11.5 Å, respectively. Both neurotransmitters consist of an aromatic ring having two oxygen atoms attached to it. The only difference in their structure is the presence of an extra oxygen atom and a methyl group in AD molecule. The optimized geometries of DA and AD adsorbed BNNRs are presented in Figure 2 and Figure 3, respectively. After the adsorption of AD on ABNNR and ZBNNR, the distance between them is 2.38 and 2.42 Å, respectively. In the case of DA on ABNNR and ZBNNR, the distance is 2.52 and 2.78 Å, respectively, as shown in Figures 2 and 3 and Table 1.

We have chosen parallel orientation for both NRTs to be adsorbed over BNNRs because planar molecules prefer parallel position due to most stable configuration.[66,72,73] In some cases, reverse of this can also be possible when there is a covalent interaction between the molecule and the surface. However,

DOI: 10.1021/acsanm.9b00028
ACS Appl. Nano Mater. 2019, 2, 1552−1561

Table 1. Calculated Energy Gap (E_g), Difference in Band Gap (ΔE_g), Adsorption Energy (E_{ad}), Distance between Molecules and BNNRs, Fermi Energy (E_F), and Work Function (Φ)[a]

	ABNNR			ZBNNR		
system	pristine	DA	AD	pristine	DA	AD
E_g (eV)	4.163	3.171	3.028	3.842	3.073	2.9
ΔE_g (eV)		0.992	1.135		0.769	0.942
E_{ad} (eV)		−1.013	−1.144		−0.701	−0.824
d (Å)		2.52	2.38		2.78	2.42
E_F (eV)	−3.061	−1.807	−1.826	−3.902	−2.083	−2.355
Φ (eV)	4.152	3.057	3.111	4.97	3.35	3.661

[a]All values are in eV.

from our previous study we know that the molecules containing aromatic ring align themselves parallel with the adsorbate, resulting higher binding energy.[66,67] In parallel position, there are more atoms to interact with the surface and also there is a chance for $\pi-\pi$ interaction between the molecule and the surface which helps to reduce the steric repulsion.[66,67,73] There is a significant change in the bond length between the boron and nitrogen atom after the adsorption of molecules due to the generation of bow (curve) on the surface of both BNNRs. The changes in the bond length along with the bond angle are presented in Table S1 of the Supporting Information. This modification in the structure of BNNRs confirms the interaction between molecules and BNNRs. Both NRTs physisorbed on BNNRs, as there is a large distance between BNNRs and molecule after the optimization which further confirms the absence of any covalent bond (chemisorption). An adsorption energy calculation is important, as it tells about the magnitude and nature of interaction between adsorbate and adsorbent (surface). Furthermore, it brings out whether the molecule is interacting with the surface or not. Using eq 1, we have calculated the adsorption energy for DA and AD over both ABNNR and ZBNNR.

The calculated adsorption energies are $E_{ad} = -1.144$ eV and $E_{ad} = -1.013$ eV for AD and DA, respectively, over ABNNR with the adsorption distance of 2.38 Å for AD and 2.52 Å for DA. Over ZBNNR the calculated adsorption energies for AD and DA are $E_{ad} = -0.824$ eV and $E_{ad} = -0.701$ eV, respectively, with the adsorption distance of 2.42 Å for AD and 2.78 Å for DA. The calculated adsorption energies reveal that the AD is strongly physisorbed over both BNNRs compared to DA which shows comparatively weak physisorption. This difference in the adsorption energy arises due to the presence of an extra oxygen atom in the AD, making it more electronegative compared to DA. A dominance of ABNNR over ZBNNR in the adsorption of NRT (DA and AD) can be attributed to the higher sensitive semiconducting nature of ABNNR toward the flow of any external charge.[74,75]

The fundamentals of binding/adsorption energy difference can be understood by van der Waals forces which depend on the size and mass of any molecule and chirality of ribbons.[76] The noncovalent adsorption energy is significantly larger compared to graphene.[55] Fernandez et al.[57] have checked the adsorption of DA over graphene with different functionals and found binding energy in the range of +0.20 to −0.94 eV which is comparatively lower than our results. However, in the case of defect created graphene the adsorption energy of DA is comparable with our results. In contrast to our results Urdaneta et al.[77] found that the DA binds covalently and chemisorbed over the TiO_2 surface. For a great drug delivery system, the molecule which is adsorbed over surface should be of physisorption type because chemisorption needs more energy to release the drug compared to physisorbed molecule which is a big drawback. This indicates that the BNNRs are good for drug release and delivery due to noncovalent interaction of both molecules. The physical nature of adsorption offers advantages in terms of easy removal and reusability of nanostructure, with no structural or electronic change in the adsorbate and adsorbent.

The main mechanism on which sensors work is the charge transfer between adsorbate and adsorbent. The significant charge transfer between the NRTs and BNNRs in the adsorption process shows that the interaction of NRTs can lead in modification of structure and electronic properties of BNNRs suitable for biosensing applications. It was found that the BNNRs adsorb NRT through physisorption to basal plane mainly driven by electromagnetic interactions (e.g., electrostatic and van der Waals).[78,79]

Figure 4 presents the molecular orbitals of both NRTs AD and DA. The HOMO−LUMO gap for AD and DA molecules

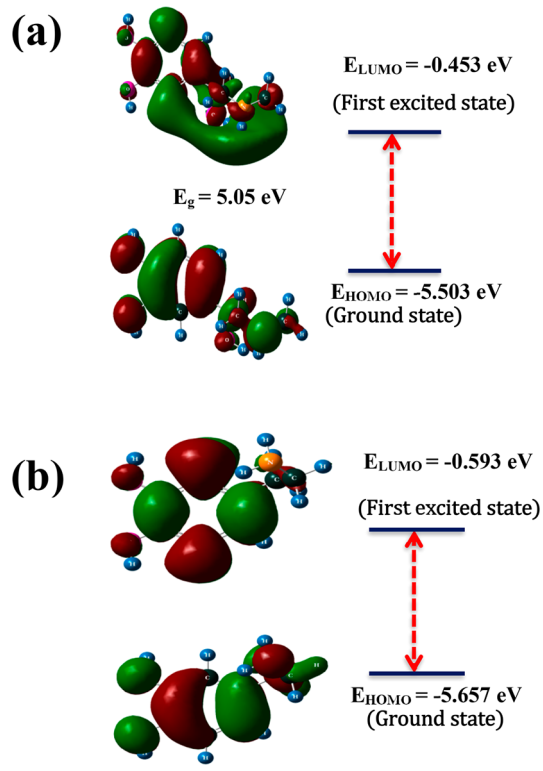

Figure 4. Molecular orbitals of (a) adrenaline and (b) dopamine.

DOI: 10.1021/acsanm.9b00028
ACS Appl. Nano Mater. 2019, 2, 1552−1561

is 5.05 and 5.064 eV, respectively. In both AD and DA, the HOMO wave functions are distributed over whole molecule as can be seen from Figure 4. The HOMO of DA shows the existence of p-orbitals on catechol ring and two hydroxyl groups making the amine group of DA less reactive. The unsaturated six-carbon ring with two hydroxyl group attached to it is termed as catechol.[80] The carbon atom consists of four valence electrons: two in 2s subshell and another two in 2p subshell. There are two unpaired electrons in 2p subshell of carbon. Molecular orbital theory describes the distribution of electrons in molecules. These p orbitals in catechol ring of DA give rise to π bonding and antibonding molecular orbitals. The side by side overlap of each two p orbitals results in the formation of two π molecular orbitals. DA shows in-phase orbitals which further results in bonding orbitals.

These significant p-orbitals can be the reason for the attraction of both ABNNR and ZBNNR resulting in the slightly bow structures. The LUMO of DA contains strong p-orbitals, as can be seen from Figure 4b that the hydroxyl groups are not so distinguishable. Similarly for the AD, the HOMO exists almost all over the catechol ring and also the nitrogen atom (Figure 4a). Conversely, the LUMO is also spread over the carbon chain. We have also calculated the total density of states (DOS) and partial density of states (PDOS) of pristine BNNRs (ABNNR and ZBNNR) and presented them in Figure 5 and Figure S1 (Supporting Information).

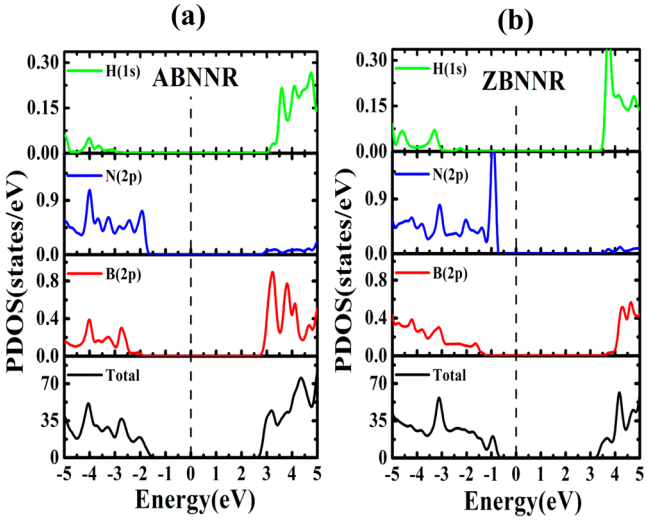

Figure 5. Total and partial DOS of (a) ABNNR and (b) ZBNNR.

These figures clearly depict wide bandgap semiconducting nature of both BNNRs. ABNNR and ZBNNR have a band gap of 4.163 and 3.842 eV, respectively.

Table 1 presents the calculated energy gap (E_g), adsorption energy (E_{ad}), Fermi energy (E_f), and distance of the adsorbed molecules from BNNRs. In ABNNR the major contribution of density in the valence band region is due to the 2p orbital participation of nitrogen atom, which falls between −2 and −10 eV while a little contribution of hydrogen atom's 1s and boron atom's 2p orbital can be seen in this area. The boron 2p orbital dominantly contributes in the conduction band region from 2 to 6 eV and in the lower valence band region near −16 to −20 eV. The trend of the contribution of orbitals in the density by nitrogen and boron is similar in ZBNNR. To further understand the effect of NRT adsorption over BNNRs system on the electronic properties of pristine BNNRs, we have calculated DOS of these systems and presented them in Figure 6 and Figure S2 (Supporting Information). Figures clearly

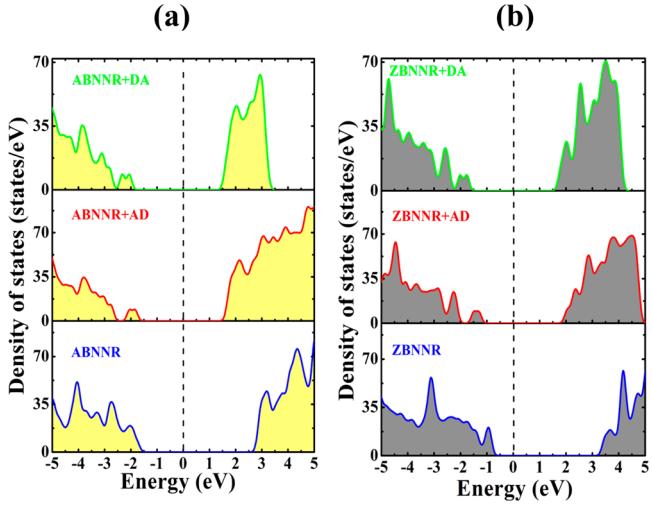

Figure 6. Density of states of (a) ABNNR adsorbed neurotransmitter and (b) ZBNNR adsorbed neurotransmitter.

depict the generation of some impurity states which are responsible for the changes in the electronic properties due to the adsorption of DA and AD molecules over both BNNRs. The adsorption of NRT reduces the band gap of both BNNRs. The decrease in the band gap by AD adsoption is more prominent than DA adsorption for both BNNRs. The extra oxygen atom in the configuration of AD may be the reason behind this large reduction compared to DA.

To have a systematic insight of the alteration of the electronic properties of BNNRs by NRT, we have calculated the PDOS for all systems and presented these in Figures 7 and 8 and Figures S3 and S4 (Supporting Information). From these figures it is clear that the contributions of both AD and DA molecules are localized at top and middle of the valence band.

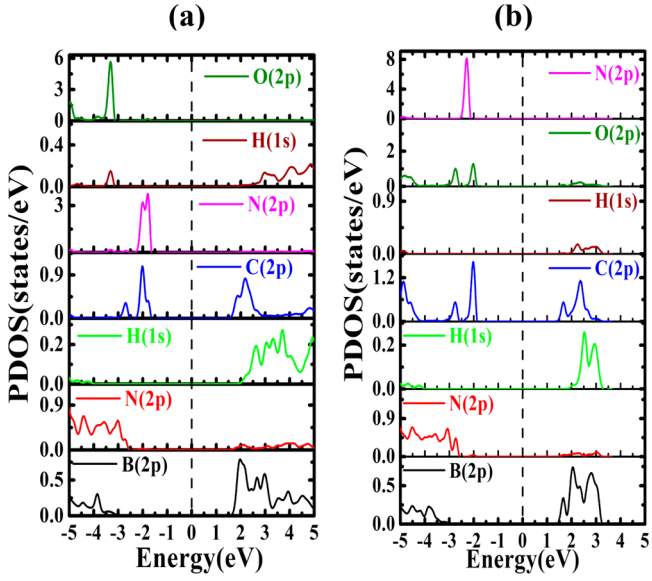

Figure 7. Partial density of states of ABNNR adsorbed with (a) adrenaline and (b) dopamine.

DOI: 10.1021/acsanm.9b00028
ACS Appl. Nano Mater. 2019, 2, 1552−1561

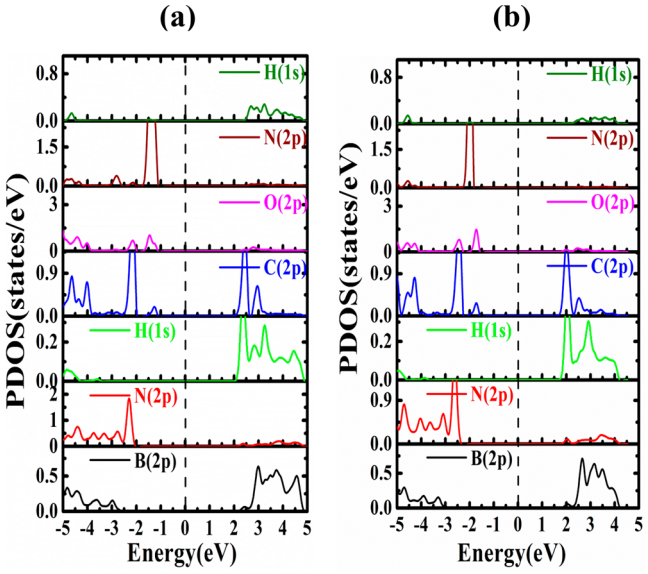

Figure 8. Partial density of states of ZBNNR adsorbed with (a) adrenaline and (b) dopamine.

For ABNNR, the states generated near the Fermi level in the valence band region are due to the p-orbital of carbon and nitrogen atoms present in AD, whereas in the case of DA, states generated are due to carbon, nitrogen, and oxygen. The lower valence band impurity states are dominated by carbon and nitrogen in AD/ABNNR, but in DA/ABNNR system lower conduction band is made by the carbon and oxygen atom's p orbital. From the PDOS plot of AD/ZBNNR and DA/ZBNNR it is clearly seen in both cases that the impurity states generated after the adsorption are due to carbon, nitrogen, and oxygen 2p states. Hence, NRTs seem to be an active unit that significantly affects electronic structure as well as electron mobility upon adsorption over BNNRs. The band gap of ABNNR reduces significantly after AD (1.135 eV) and DA (0.992 eV) adsorption. Similarly in ZBNNR, the reduction in the band gap by AD is 0.942 eV and by DA is 0.769 eV.

The large band gap modulation of ABNNR due to AD is because of the presence of extra OH group which is absent in DA. An extra oxygen atom in the AD makes it more electronegative as compared to DA resulting in the dominant adsorption of AD than DA in both cases of BNNR and is also responsible for the large modulation in the band gap. These results reinforce the fact that the molecules get physically adsorbed on the nanosurface of both BNNRs indicating their suitability for the targeted delivery of the molecule as reversibility of the nanoribbon can be easily achieved by the desorption. We further analyzed the electron transport by calculating the Lowdin charge transfer. The significant charge transfer between the NRT (AD and DA) and both BNNRs is observed after the adsorption process which can be the reason for the modification in structural and electronic properties of BNNRs. There is a charge transfer of 0.15*e* and 0.10*e*, respectively, in the cases of AD and DA adsorbed over ABNNR and 0.12*e* and 0.10*e*, respectively, for AD and DA adsorbed over ZBNNR. Figure S5 (Supporting Information) shows the calculated charge density counter.

The effect on the electronic properties of any surface after adsorption further can be confirmed from the electrical conductivity (σ) which can be evaluated using energy gap E_g, an important electronic parameter for a material. The electrical conductivity σ can be evaluated by the following classic expression[81]

$$\sigma \propto e^{-E_g/(2KT)} \tag{2}$$

where K and T are the Boltzmann's constant and temperature, respectively. According to eq 2, conductivity is inversely proportional to the bandgap, which means the smaller the value of bandgap E_g, higher is the electrical conductivity at given temperature T. Thus, adsorption of NRTs over both BNNRs surface which significantly decreases the band gap increases the electrical conductivity σ of the BNNRs. For both ABNNR and ZBNNR the trend of σ enhancement is more for AD than DA (AD > DA), which means AD adsorption enhances conductivity more than the DA adsorption. The change in the Fermi level of BNNRs due to the adsorption of NRT molecules causes an electrical signal, and therefore it could potentially be used in biosensor applications.

The change in the electronic properties of BNNRs by the adsorption of NRT (AD and DA) can be further understood from the value of the work function (WF).[9,81] We have calculated the WF using first-principles calculations. The work function is the amount of energy required by an electron to get free from Fermi level of any material to vacuum level which can be expressed by the following equation:[81]

$$\mathrm{WF}(\Phi) = E_{\mathrm{vac}} - E_{\mathrm{F}} \tag{3}$$

where E_{vac} denotes the energy of vacuum level and E_{F} denotes the energy of Fermi level. The calculated work functions are shown in Figure 9. The distance of the molecule from the surface can be understood by the position of the peak in the graph.

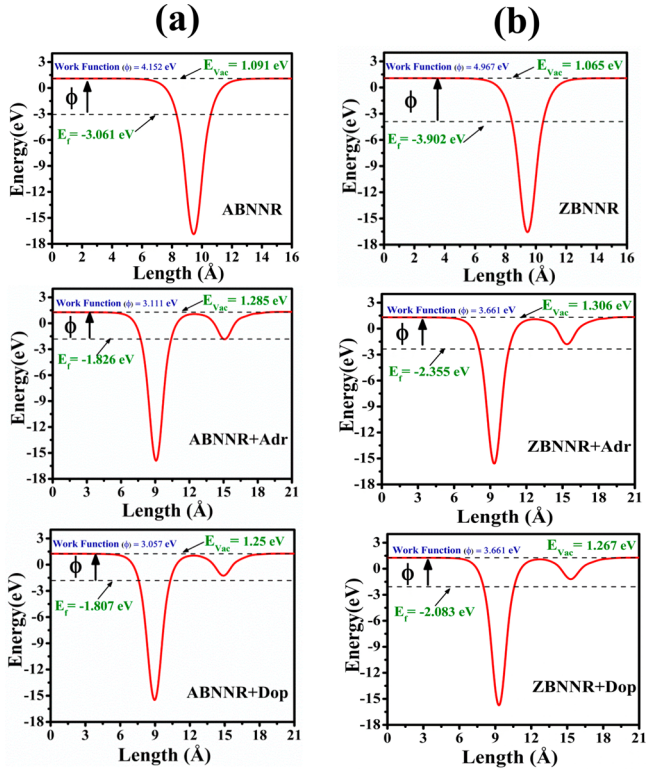

Figure 9. Work function of BNNR and neurotransmitter adsorbed (a) ABNNR and (b) ZBNNR.

DOI: 10.1021/acsanm.9b00028
ACS Appl. Nano Mater. 2019, 2, 1552−1561

After the adsorption of NRT on both BNNRs a dramatic change in the work function is observed. The work function reduces by 26% and 32% after the adsorption of AD and DA over ZBNNR while same reduces by 25% and 26% after the adsorption of AD and DA over ABNNR. The significant change in the work function of ZBNNR is due to its structural asymmetry and hydrogen passivation which possesses a permanent transverse dipole moment,[19] and further both dipole moment and work function are related to each other.[82] The distinct alteration of work function WF(Φ) after the adsorption of AD and DA NRTs (through strong physisorption) indicates a strong influence of these molecules on the BNNRs surface.

CONCLUSION

Stressful lifestyle leads to many cerebral diseases in the society, caused by the imbalance in the neurotransmitters present in the brain. Neurotransmitters being the most essential chemical of brain have ability to maintain the cognitive as well as synaptic functions in all mammals including humans. The detection and maintenance of the neurotransmitter level in human body are of utmost importance. However, the requirement of controlled environment and expensive method creates challenges in monitoring the neurotransmitter level. A simple and highly sensitive electrochemical sensor can ease the detection and monitoring process. Boron nitride nanoribbons (BNNRs) are emerging noncytotoxic materials suitable for biomolecule's detection and their transport. In our work, we have performed a detailed investigation on the interaction of two important neurotransmitters, namely, DA and AD adsorbed over armchair and zigzag BNNR with the help of density functional theory based abinitio calculations. Our results suggest that BNNRs are capable of detecting and carrying the neurotransmitter. According to the calculated adsorption energies and structural analysis, both DA and AD were physisorbed on ABNNR and ZBNNR. The functionalization of planar BNNRs with NRTs results in the formation of slightly arched (curved) structure of BNNR. Through the comparative study of NRTs over BNNRs, our study reveals that the ABNNR shows strong noncovalent interaction with DA and AD compared to another study which can be attributed to its semiconducting behavior. To the best of our knowledge, BNNR as NRT carrier is yet to be developed experimentally. We hope that the efforts will be directed toward developing and accessing the viability of BNNR based biosensor and drug delivery system for neurotransmitter carrier. We believe that the present study will help the experimentalists to develop neurotransmitter carrier based on BNNR.

ASSOCIATED CONTENT

Supporting Information

The Supporting Information is available free of charge on the ACS Publications website at DOI: 10.1021/acsanm.9b00028.

Calculated bond angle and bond length of BNNRs after adsorption of NRT, full range DOS and PDOS of ABNNR and ZBNNR, full DOS of ABNNR and ZBNNR adsorbed NRT, PDOS of ABNNR adsorbed with AD and DA, PDOS of ZBNNR adsorbed with AD and DA, charge density contour of NRT adsorbed ABNNR and ZBNNR (PDF)

AUTHOR INFORMATION

Corresponding Author

*E-mail: prafullaj@yahoo.com; pk.jha-phy@msubaroda.ac.in. Telephone: +91-265-2795339.

ORCID

Prafulla K Jha: 0000-0002-9358-3940

Author Contributions

B.R and P.K.J. have contributed equally.

Notes

The authors declare no competing financial interest.

ACKNOWLEDGMENTS

The study is financially supported by a research project from Science and Engineering Research Board (SERB) (Grant SR/S2/CMP-0005/2013), Government of India. The computations were carried out using high performance computer cluster provided under the DST-FIST program.

REFERENCES

(1) Geim, A. K.; Novoselov, K. S. The Rise of Graphene. *Nat. Mater.* **2007**, *6*, 183−191.

(2) Novoselov, K. S.; Geim, A. K.; Morozov, S. V.; Jiang, D.; Katsnelson, M. I.; Grigorieva, I. V.; Dubonos, S. V.; Firsov, A. A. Two-dimensional gas of massless Dirac fermions in graphene. *Nature* **2005**, *438*, 197−200.

(3) Novoselov, K. S.; Geim, A. K.; Morozov, S. V.; Jiang, D.; Zhang, Y.; Dubonos, S. V.; Grigorieva, I. V.; Firsov, A. A. Electric Field Effect in Atomically Thin Carbon Films. *Science* **2004**, *306*, 666−669.

(4) Potyrailo, R. A.; Surman, C.; Nagraj, N.; Burns, A. Materials and Transducers Toward Selective Wireless Gas Sensing. *Chem. Rev.* **2011**, *111*, 7315−7354.

(5) Song, X.; Hu, J.; Zeng, H. Two-Dimensional Semiconductors : Recent Progress and Future Prespectives. *J. Mater. Chem. C* **2013**, *1*, 2952−2969.

(6) Costa, A. L. M. T.; Silva, F. W. N.; Barros, E. B. Spin Polarized Vertical Transport in Stacked TMDCs Hetero-Junctions. *Semicond. Sci. Technol.* **2018**, *33*, 075018−075025.

(7) Liu, H.; Neal, A. T.; Zhu, Z.; Luo, Z.; Xu, X.; Tománek, D.; Ye, P. D. Phosphorene : An Unexplored 2D Semiconductor with a High Hole. *ACS Nano* **2014**, *8*, 4033−4041.

(8) Cahangirov, S.; Topsakal, M.; Akturk, E.; Sahin, H.; Ciraci, S. Two- and One-Dimensional Honeycomb Structures of Silicon and Germanium. *Phys. Rev. Lett.* **2009**, *102*, 236804.

(9) Patel, K.; Roondhe, B.; Dabhi, S. D.; Jha, P. K. A New Flatland Buddy as Toxic Gas Scavenger: A First Principles Study. *J. Hazard. Mater.* **2018**, *351*, 337−345.

(10) Rubio, A.; Corkill, J. L.; Cohen, M. L. Theory of Graphitic Boron Nitride Nanotubes. *Phys. Rev. B: Condens. Matter Mater. Phys.* **1994**, *49*, 5081−5084.

(11) Singla, P.; Riyaz, M.; Singhal, S.; Goel, N. Theoretical Study of Adsorption of Amino Acids on Graphene and BN Sheet in Gas and Aqueous Phase Including Empirical DFT Dispersion Correction. *Phys. Chem. Chem. Phys.* **2016**, *18*, 5597−5604.

(12) Saghayimarouf, N.; Monajjemi, M. QM/MM Study of Methamphetamine and Dopamine Adsorption on SWCNTs and SWBNNTs. *J. Comput. Theor. Nanosci.* **2017**, *14*, 957−964.

(13) Topsakal, M.; Aktürk, E.; Ciraci, S. First-Principles Study of Two- and One-Dimensional Honeycomb Structures of Boron Nitride. *Phys. Rev. B: Condens. Matter Mater. Phys.* **2009**, *79*, 115442−115452.

(14) Muramatsu, Y.; Kaneyoshi, T.; Gullikson, E. M.; Perera, R. C. C. Angle-Resolved Soft X-Ray Emission and Absorption Spectroscopy of Hexagonal Boron Nitride. *Spectrochim. Acta, Part A* **2003**, *59*, 1951−1957.

(15) Zeng, H.; Zhi, C.; Zhang, Z.; Wei, X.; Wang, X.; Guo, W.; Bando, Y.; Golberg, D. "White Graphenes": Boron Nitride Nanorib-

DOI: 10.1021/acsanm.9b00028
ACS Appl. Nano Mater. 2019, 2, 1552−1561

bons via Boron Nitride Nanotube Unwrapping. *Nano Lett.* **2010**, *10*, 5049−5055.
(16) Erickson, K. J.; Gibb, A. L.; Sinitskii, A.; Rousseas, M.; Alem, N.; Tour, J. M.; Zettl, A. K. Longitudinal Splitting of Boron Nitride Nanotubes for the Facile Synthesis of High Quality Boron Nitride Nanoribbons. *Nano Lett.* **2011**, *11*, 3221−3226.
(17) Zheng, F.; Zhou, G.; Liu, Z.; Wu, J.; Duan, W.; Gu, B.-L.; Zhang, S. B. Half Metallicity along the Edge of Zigzag Boron Nitride Nanoribbons. *Phys. Rev. B: Condens. Matter Mater. Phys.* **2008**, *78*, 205415−205419.
(18) Lai, L.; Lu, J.; Wang, L.; Luo, G.; Zhou, J.; Qin, R.; Gao, Z.; Mei, W. N. Magnetic Properties of Fully Bare and Half-Bare Boron Nitride Nanoribbons. *J. Phys. Chem. C* **2009**, *113*, 2273−2276.
(19) Qi, J.; Qian, X.; Qi, L.; Feng, J.; Shi, D.; Li, J. Strain-Engineering of Band Gaps in Piezoelectric Boron Nitride Nanoribbons. *Nano Lett.* **2012**, *12*, 1224−1228.
(20) Zhu, S.; Li, T. Strain-induced programmable half-metal and spin-gapless semiconductor in an edge-doped boron nitride nanoribbon. *Phys. Rev. B: Condens. Matter Mater. Phys.* **2016**, *93*, 115401.
(21) Zhang, Z.; Liu, X.; Yu, J.; Hang, Y.; Li, Y.; Guo, Y.; Xu, Y.; Sun, X.; Zhou, J.; Guo, W. Tunable electronic and magnetic properties of two-dimensional materials and their one-dimensional derivatives. *WIREs. Comput. Mol. Sci.* **2016**, *6*, 324−350.
(22) Algharagholy, L.; Pope, T. W. D.; Bailey, S.; Lambert, C. J. Electronic properties of sculpturenes. *New J. Phys.* **2014**, *16*, 013060−013082.
(23) Lopez-Bezanilla, A.; Huang, J.; Terrones, H.; Sumpter, B. G. Structure and Electronic Properties of Edge-Functionalized Armchair Boron Nitride Nanoribbons. *J. Phys. Chem. C* **2012**, *116*, 15675−15681.
(24) Pan, H.; Zhang, Y.-W. Tuning the electronic properties of MoS2 nanoribbons by strain engineering. *J. Phys. Chem. C* **2012**, *116*, 11752−11757.
(25) Song, L. L.; Zheng, X. H.; Hao, H.; Lan, J.; Wang, X. L.; Zeng, Z. Tuning the electronic and magnetic properties in zigzag boron nitride nanoribbons with carbon dopants. *Comput. Mater. Sci.* **2014**, *81*, 551−555.
(26) Jin, L.; Li-Zhong, S.; Jian-Xin, Z. Strain Effects on Electronic Properties of Boron Nitride Nanoribbons. *Chin. Phys. Lett.* **2010**, *27*, 077101.
(27) Feng, C.; ChenYuan-Ping; Mi, Z.; Jian-Xin, Z. Strain effect on transport properties of hexagonal boron−nitride nanoribbons. *Chin. Phys. B* **2010**, *19*, 086105.
(28) Chen, X.; Wu, P.; Rousseas, M.; Okawa, D.; Gartner, Z.; Zettl, A.; Bertozzi, C. R. Boron Nitride Nanotubes Are Noncytotoxic and Can Be Functionalized for Interaction with Proteins and Cells. *J. Am. Chem. Soc.* **2009**, *131*, 890−891.
(29) Danti, S.; Ciofani, G.; Moscato, S.; D'Alessandro, D.; Ciabatti, E.; Nesti, C.; Brescia, R.; Bertoni, G.; Pietrabissa, A.; Lisanti, M.; Petrini, M.; Mattoli, V.; Berrettini, S. Boron nitride nanotubes and primary human osteoblasts: in vitro compatibility and biological interactions under low frequency ultrasound stimulation. *Nanotechnology* **2013**, *24*, 465102−465114.
(30) Jiang, X.; Weng, Q.; Wang, X.; Li, X.; Zhang, J.; Golberg, D.; Bando, Y. Recent Progress on Fabrications and Applications of Boron Nitride Nanomaterials: A Review. *J. Mater. Sci. Technol.* **2015**, *31*, 589−598.
(31) Merlo, A.; Mokkapati, V. R. S. S.; Pandit, S.; Mijakovic, I. Boron nitride nanomaterials: biocompatibility and bio-applications. *Biomater. Sci.* **2018**, *6*, 2298−2311.
(32) Mateti, S.; Wong, C. S.; Liu, Z.; Yang, W.; Li, Y.; Li, L. H.; Chen, Y. Biocompatibility of boron nitride nanosheets. *Nano Res.* **2018**, *11*, 334−342.
(33) Jackowska, K.; Krysinski, P. New Trends in the Electrochemical Sensing of Dopamine. *Anal. Bioanal. Chem.* **2013**, *405*, 3753−3771.
(34) Mele, T.; Čarman-Kržan, M.; Juričˇ, D. M. Regulatory Role of Monoamine Neurotransmitters in Astrocytic NT-3 Synthesis. *Int. J. Dev. Neurosci.* **2010**, *28*, 13−19.
(35) Lövheim, H. A New Three-Dimensional Model for Emotions and Monoamine Neurotransmitters. *Med. Hypotheses* **2012**, *78*, 341−348.
(36) Mo, J. W.; Ogorevc, B. Simultaneous Measurement of Dopamine and Ascorbate at Their Physiological Levels Using Voltammetric Microprobe Based on Overoxidized Poly(1,2-Phenylenediamine)-Coated Carbon Fiber. *Anal. Chem.* **2001**, *73*, 1196−1202.
(37) Galvan, A.; Wichmann, T. Pathophysiology of Parkinsonism. *Clin. Neurophysiol.* **2008**, *119*, 1459−1474.
(38) Mohammadi, M.; Akhondzadeh, S. Advances and Considerations in Attention-Deficit/Hyperactivity Disorder Pharmacotherapy. *Acta Med. Iran.* **2011**, *49*, 487−498.
(39) Obata, T. Dopamine Efflux by MPTP and Hydroxyl Radical Generation. *J. Neural Transm.* **2002**, *109*, 1159−1180.
(40) Song, Y. Theoretical Study on the Electrochemical Behavior of Norepinephrine at Nafion Multi-Walled Carbon Nanotubes Modified Pyrolytic Graphite Electrode. *Spectrochim. Acta, Part A* **2007**, *67*, 1169−1177.
(41) Baron, R.; Zayats, M.; Willner, I. Dopamine-, L-DOPA-, Adrenaline-, and Noradrenaline-Induced Growth of Au Nanoparticles : Assays for the Detection of Neurotransmitters and of Tyrosinase Activity. *Anal. Chem.* **2005**, *77*, 1566−1571.
(42) Chen, S. M.; Peng, K. T. The Electrochemical Properties of Dopamine, Epinephrine, Norepinephrine, and Their Electrocatalytic Reactions on Cobalt(II) Hexacyanoferrate Films. *J. Electroanal. Chem.* **2003**, *547*, 179−189.
(43) Perati, P. R.; Cheng, J.; Jandik, P.; Hanko, V. P. Disposable Carbon Electrodes for Liquid Chromatographic Detection of Catecholamines in Blood Plasma Samples. *Electroanalysis* **2010**, *22*, 325−332.
(44) Chen, J.; Zhang, J.; Lin, X.; Wan, H.; Zhang, S. Electrocatalytic Oxidation and Determination of Dopamine in the Presence of Ascorbic Acid and Uric Acid at a Poly (4-(2-Pyridylazo)-Resorcinol) Modified Glassy Carbon Electrode. *Electroanalysis* **2007**, *19*, 612−615.
(45) Dong, H.; Wang, S.; Liu, A.; Galligan, J. J.; Swain, G. M. Drug Effects on the Electrochemical Detection of Norepinephrine with Carbon Fiber and Diamond Microelectrodes. *J. Electroanal. Chem.* **2009**, *632*, 20−29.
(46) Łuczak, T. Electroanalysis of Norepinephrine at Bare Gold Electrode Pure and Modified with Gold Nanoparticles and S-Functionalized Self-Assembled Layers in Aqueous Solution. Part II. *Electroanalysis* **2010**, *22*, 2641−2649.
(47) Yao, H.; Li, S.; Tang, Y.; Chen, Y.; Chen, Y.; Lin, X. Selective Oxidation of Serotonin and Norepinephrine over Eriochrome Cyanine R Film Modified Glassy Carbon Electrode. *Electrochim. Acta* **2009**, *54*, 4607−4612.
(48) Zare, H. R.; Nasirizadeh, N. Simultaneous Determination of Ascorbic Acid, Adrenaline and Uric Acid at a Hematoxylin Multi-Wall Carbon Nanotube Modified Glassy Carbon Electrode. *Sens. Actuators, B* **2010**, *143*, 666−672.
(49) Viry, L.; Derré, A.; Poulin, P.; Kuhn, A. Discrimination of Dopamine and Ascorbic Acid Using Carbon Nanotube Fiber Microelectrodes. *Phys. Chem. Chem. Phys.* **2010**, *12*, 9993−9995.
(50) Zeng, B.; Yang, Y.; Zhao, F. Voltammetric Determination of Epinephrine with a 3- Mercaptopropionic Acid Self-Assembled Monolayer Modified Gold Electrode. *Electroanalysis* **2003**, *15*, 1054−1059.
(51) Fotopoulou, M. A.; Ioannou, P. C. Post-Column Terbium Complexation and Sensitized Fluorescence Detection for the Determination of Norepinephrine, Epinephrine and Dopamine Using High-Performance Liquid Chromatography. *Anal. Chim. Acta* **2002**, *462*, 179−185.
(52) Britz-Mckibbin, P.; Wong, J.; Chen, D. D. Y. Analysis of Epinephrine from Fifteen Different Dental Anesthetic Formulations by Capillary Electrophoresis. *J. Chromatogr. A* **1999**, *853*, 535−540.

DOI: 10.1021/acsanm.9b00028
ACS Appl. Nano Mater. 2019, 2, 1552−1561

(53) Su, Y.; Wang, J.; Chen, G. Determination of Epinephrine Based on its Enhancement for Electrochemiluminescence of Lucigenin. *Talanta* **2005**, *65*, 531−536.
(54) Kamidate, T.; Kaide, T.; Tani, H.; Makino, E.; Shibata, T. Effect of Mixing Modes on Chemiluminescent Detection of Epinephrine with Lucigenin by an FIA System Fabricated on a Microchip. *Anal. Sci.* **2001**, *17*, 951−955.
(55) Ortiz-Medina, J.; López-Urías, F.; Terrones, H.; Rodríguez-Macías, F. J.; Endo, M.; Terrones, M. Differential Response of Doped/Defective Graphene and Dopamine to Electric Fields: A Density Functional Theory Study. *J. Phys. Chem. C* **2015**, *119*, 13972−13978.
(56) Feng, X.; Zhang, Y.; Zhou, J.; Li, Y.; Chen, S.; Zhang, L.; Ma, Y.; Wang, L.; Yan, X. Three-Dimensional Nitrogen-Doped Graphene as an Ultrasensitive Electrochemical Sensor for the Detection of Dopamine. *Nanoscale* **2015**, *7*, 2427−2432.
(57) Rossi Fernández, A. C.; Castellani, N. J. Noncovalent Interactions between Dopamine and Regular and Defective Graphene. *ChemPhysChem* **2017**, *18*, 2065−2080.
(58) Khan, A. F.; Brownson, D. A. C.; Foster, C. W.; Smith, G. C.; Banks, C. E. Surfactant Exfoliated 2D Hexagonal Boron Nitride (2D-hBN) Explored as a Potential Electrochemical Sensor for Dopamine: Surfactants Significantly Influence Sensor Capabilities. *Analyst* **2017**, *142*, 1756−1764.
(59) Giannozzi, P.; Baroni, S.; Bonini, N.; Calandra, M.; Car, R.; Cavazzoni, C.; Ceresoli, D.; Chiarotti, G. L.; Cococcioni, M.; Dabo, I.; Dal Corso, A.; Fabris, S.; Fratesi, G.; de Gironcoli, S.; Gebauer, R.; Gerstmann, U.; Gougoussis, C.; Kokalj, A.; Lazzeri, M.; Martin-Samos, L.; Marzari, N.; Mauri, F.; Mazzarello, R.; Paolini, S.; Pasquarello, A.; Paulatto, L.; Sbraccia, C.; Scandolo, S.; Sclauzero, G.; Seitsonen, A. P.; Smogunov, A.; Umari, P.; Wentzcovitch, R. M. QUANTUM ESPRESSO: A Modular and Open-Source Software Project for Quantum Simulations of Materials. *J. Phys.: Condens. Matter* **2009**, *21*, 395502.
(60) Head, J. D.; Zerner, M. C. A Broyden-Fletcher-Goldfarb-Shanno Optimization Procedure for Molecular Geometries. *Chem. Phys. Lett.* **1985**, *122*, 264−270.
(61) Perdew, J. P.; Burke, K.; Ernzerhof, M. Generalized Gradient Approximation Made Simple. *Phys. Rev. Lett.* **1996**, *77*, 3865−3868.
(62) Favot, F.; Dal Corso, A.; Baldereschi, A. CO adsorbed on Cu(001): A comparison between local density approximation and Perdew, Burke, and Ernezerhof generalized gradient approximation. *J. Chem. Phys.* **2001**, *114*, 483−488.
(63) Juan, Y. M.; Kaxiras, E.; Gordon, R. G. Use of the generalized gradient approximation in pseudopotential calculations of solids. *Phys. Rev. B: Condens. Matter Mater. Phys.* **1995**, *51*, 9521−9525.
(64) Monkhorst, H. J.; Pack, J. D. Special Points for Brillouin Zone Integrations. *Phys. Rev. B* **1976**, *13*, 5188−5192.
(65) Corno, M.; Rimola, A.; Bolis, V.; Ugliengo, P. Hydroxyapatite as a Key Biomaterial: Quantum-Mechanical Simulation of its Surfaces in Interaction with Biomolecules. *Phys. Chem. Chem. Phys.* **2010**, *12*, 6309−6329.
(66) Dabhi, S. D.; Roondhe, B.; Jha, P. K. Nucleobases-Decorated Boron Nitride Nanoribbons for Electrochemical Biosensing: A Dispersion-Corrected DFT Study. *Phys. Chem. Chem. Phys.* **2018**, *20*, 8943−8950.
(67) Roondhe, B.; Dabhi, S. D.; Jha, P. K. Sensing Properties of Pristine Boron Nitride Nanostructures towards Alkaloids : A First Principles Dispersion Corrected Study. *Appl. Surf. Sci.* **2018**, *441*, 588−598.
(68) Grimme, S. Semiempirical GGA-Type Density Functional Constructed with a Long-Range Dispersion Correction. *J. Comput. Chem.* **2006**, *27*, 1787−1799.
(69) Davis, J. B. A.; Baletto, F.; Johnston, R. L. The Effect of Dispersion Correction on the Adsorption of CO on Metallic Nanoparticles. *J. Phys. Chem. A* **2015**, *119*, 9703−9709.
(70) Krukau, A. V.; Vydrov, O. A.; Izmaylov, A. F.; Scuseria, G. E. Influence of the Exchange Screening Parameter on the Performance of Screened Hybrid Functionals. *J. Chem. Phys.* **2006**, *125* (22), 224106−224111.
(71) Frisch, M. J.; Trucks, G. W.; Schlegel, H. B.; Scuseria, G. E.; Robb, M. A.; Cheeseman, J. R.; Scalmani, G.; Barone, V.; Mennucci, B.; Petersson, G. A.; Nakatsuji, H.; Caricato, M.; Li, X.; Hratchian, H. P.; Izmaylov, A. F.; Bloino, J.; Zheng, G.; Sonnenberg, J. L.; Hada, M.; Ehara, M.; Toyota, K.; Fukuda, R.; Hasegawa, J.; Ishida, M.; Nakajima, T.; Honda, Y.; Kitao, O.; Nakai, H.; Vreven, T.; Montgomery, J. A.; Peralta, J. E.; Ogliaro, F.; Bearpark, M.; Heyd, J. J.; Brothers, E.; Kudin, K. N.; Staroverov, V. N.; Keith, T.; Kobayashi, R.; Normand, J.; Raghavachari, K.; Rendell, A.; Burant, J. C.; Iyengar, S. S.; Tomasi, J.; Cossi, M.; Rega, N.; Millam, J. M.; Klene, M.; Knox, J. E.; Cross, J. B.; Bakken, V.; Adamo, C.; Jaramillo, J.; Gomperts, R.; Stratmann, R. E.; Yazyev, O.; Austin, A. J.; Cammi, R.; Pomelli, C.; Ochterski, J. W.; Martin, R. L.; Morokuma, K.; Zakrzewski, V. G.; Voth, G. A.; Salvador, P.; Dannenberg, J. J.; Dapprich, S.; Daniels, A. D.; Farkas, O.; Foresman, J. B.; Ortiz, J. V.; Cioslowski, J.; Fox, D. J. *Gaussian 09*, revision D.01; Gaussian Inc.: Wallingford, CT, 2010.
(72) Anota, E. C.; Tlapale, Y.; Villanueva, M. S.; Márquez, J. A. R. Non-Covalent Functionalization of Hexagonal Boron Nitride Nanosheets with Guanine. *J. Mol. Model.* **2015**, *21*, 215−220.
(73) Roondhe, B.; Jha, P. K. "Haeckelite", a New Low Dimensional Cousin of Boron Nitride for Biosensing with Ultra-Fast Recovery Time : A First Principles Investigation. *J. Mater. Chem. B* **2018**, *6*, 6796−6807.
(74) Park, C.-H.; Louie, S. G. Energy Gaps and Stark Effect in Boron Nitride Nanoribbons. *Nano Lett.* **2008**, *8*, 2200−2203.
(75) Zhang, Z.; Guo, W. Energy-Gap Modulation of BN Ribbons by Transverse Electric Fields : First-Principles Calculations. *Phys. Rev. B: Condens. Matter Mater. Phys.* **2008**, *77*, 075403−075407.
(76) Han, P.; Akagi, K.; Canova, F. F.; Mutoh, H.; Shiraki, S.; Iwaya, K.; Weiss, P. S.; Asao, N.; Hitosugi, T. Bottom-Up Graphene-Nanoribbon Fabrication Reveals Chiral Edges and Enantioselectivity. *ACS Nano* **2014**, *8*, 9181−9187.
(77) Urdaneta, I.; Keller, A.; Atabek, O.; Palma, J. L.; Finkelstein-Shapiro, D.; Tarakeshwar, P.; Mujica, V.; Calatayud, M. Dopamine Adsorption on TiO2 Anatase Surfaces. *J. Phys. Chem. C* **2014**, *118*, 20688−20693.
(78) Moses, P. G.; Mortensen, J. J.; Lundqvist, B. I.; Nørskov, J. K. Density functional study of the adsorption and van der Waals binding of aromatic and conjugated compounds on the basal plane of MoS2. *J. Chem. Phys.* **2009**, *130*, 104709−104714.
(79) Berland, K.; Hyldgaard, P. Analysis of van der Waals density functional components: Binding and corrugation of benzene and C60 on boron nitride and graphene. *Phys. Rev. B: Condens. Matter Mater. Phys.* **2013**, *87*, 205421−205435.
(80) Norris, D. O.; Carr, J. A. *Synthesis, Metabolism, and Actions of Bioregulators*; Vertebrate Endocrinology; Academic Press, 2013; 41−91.
(81) Li, S. S.. *Semiconductor Physical Electronics*, 2nd ed.; Springer Science & Business Media, 2006.
(82) Saito, Y.; Yada, K.; Minami, K.; Nakane, H.; Adachi, H. Experimental relationship between work function and dipole moment on Er O/W (100) and Lu O/W (100) emitter surfaces. *J. Vac. Sci. Technol., B: Microelectron. Process. Phenom.* **2004**, *22*, 2743−2747.

DOI: 10.1021/acsanm.9b00028
ACS Appl. Nano Mater. 2019, 2, 1552−1561